Lack of an atypical PDR transporter generates an immunogenic *Cryptococcus neoformans* strain that drives a dysregulated and lethal immune response in murine lungs

Christopher J. Winski[1], Peter V. Stuckey[1], Armando M. Marrufo[1], Robbi L. Ross[1,2], Georgina Agyei[1], Sarah Chapman[5], and Felipe H. Santiago-Tirado[1,2,3,4,#]

[1] Department of Biological Sciences, University of Notre Dame, Notre Dame, Indiana, USA

[2] Integrated Biomedical Sciences, University of Notre Dame, Notre Dame, Indiana, USA

[3] Eck Institute for Global Health, University of Notre Dame, Notre Dame, Indiana, USA

[4] Warren Center for Drug Discovery, University of Notre Dame, Notre Dame, Indiana, USA

[5] Integrated Imaging Facility, University of Notre Dame, Notre Dame, Indiana, USA

Running Head: PDR transporter role during cryptococcal infection

#Address correspondence to Felipe H. Santiago-Tirado, fsantiago@nd.edu

Word Counts

Abstract: 215

Importance: 149

Text (excluding Methods, References, and captions): 5,836

ABSTRACT

Cryptococcus neoformans is an opportunistic fungal pathogen responsible for >150,000 deaths every year with a mortality rate as high as 81%. This high medical burden is due, in part, to an incomplete understanding of its pathogenesis. In a previous study, we identified a cryptococcal atypical pleiotropic drug resistance (PDR) transporter, *PDR6*, that regulated antifungal resistance and host interactions. Here, we follow-up on the role of *PDR6* in cryptococcal virulence. *In vivo*, mice infected with the *pdr6*Δ strain display altered symptomatology and disease progression. Specifically, we observed a significant increase in the innate immune cell populations in the *pdr6*Δ-infected mice when compared to their WT-infected littermates. Furthermore, quantification of pulmonary cytokines/chemokines revealed a robust increase of pro-inflammatory cytokines in mice infected with the *pdr6*Δ mutant strain. Whereas antifungal treatment of *pdr6*Δ-infected animals did not affect survival, treatment with a corticosteroid significantly extended survival, highlighting the importance of a balanced/controlled host immune response. We determined that the hyper-inflammatory immune response occurs, in part, because the loss of the Pdr6 transporter indirectly alters the cryptococcal cell wall architecture and results in the increased exposure of chitin, β-glucan, and other cryptococcal-specific pathogen associated molecular patterns. Taken together, this study provides clinical insights regarding cryptococcal pathogenesis while also providing additional functions of PDR-type ATP-binding cassette (ABC) transporters in pathogenic fungi.

42 **IMPORTANCE**

43 Yeasts of the *Cryptococcus* genus, especially *C. neoformans*, can cause disease with unacceptably
44 high mortality. This is due to delays in diagnostics, ineffective treatments, and an incomplete
45 understanding of the interactions between this fungus and our immune system. In this study, we
46 expand our knowledge of the biological function of the *PDR6* gene, particularly its effect on
47 modulating the host's immune response. Normally, *C. neoformans*'s infections are characterized
48 by an anti-inflammatory response that is unable to control the yeast. In the absence of *PDR6*, the
49 response to the infection is a dysregulated pro-inflammatory response that initially controls the
50 fungi but eventually results in death of the host due to too much tissue damage. This is due, in
51 part, to an altered fungal surface. Given the dual role of *PDR6* in modulating antifungal sensitivity
52 and immune responses, this work provides important insights that may lead to new or improved
53 therapeutics.

54 **INTRODUCTION**

55 Commonly associated with soil and bird guano, *Cryptococcus neoformans* is an
56 environmental, opportunistic yeast responsible for >194,000 infections every year (1). Upon
57 inhalation of spores or desiccated yeast, *C. neoformans* reaches the alveoli where it encounters
58 alveolar macrophages and other host immune cells (2); however, this fungus is capable of
59 establishing a unique intracellular niche that allows it to survive and replicate within these host
60 cells (3). The neurotropic fungus can then disseminate to extrapulmonary organs, traverse the
61 blood-brain-barrier and enter the central nervous system (CNS), resulting in cryptococcal
62 meningoencephalitis (CME) with a mortality rate as high as 81% (1, 4, 5). Several lines of evidence
63 indicate that in addition to its use of host immune cells as replication havens, *C. neoformans* can
64 use infected cells as vehicles for dissemination and brain invasion (5, 6). Hence, understanding
65 this complex cryptococcal-phagocyte interaction from both fungal and host perspectives
66 represents a challenging but clinically relevant avenue of research given its role in determining
67 the course and outcome(s) of infection.

68 In addition to its ability to survive intracellularly, *C. neoformans* has several other
69 virulence factors including an antiphagocytic polysaccharide capsule that provides protection
70 from host stressors and masks several cryptococcal pathogen-associated molecular patterns
71 (PAMPs) including chitin, chitosan, mannoproteins, and β-glucans from host phagocytes (7).
72 Structurally composed of glucuronoxylomannan (GXM) and glucuronoxylomannogalactan
73 (GXMGal), the capsule is also constitutively secreted/shed and it modulates the host immune
74 response in ways that promote infection (8). Additionally, *C. neoformans* synthesizes cell wall-
75 localized melanin that protects the yeast from ultraviolet radiation and oxidative/nitrosative

76 stress. Finally, the fungus displays thermotolerance, able to grow at physiological-relevant
77 conditions (37°C + 5% CO_2) (9-11). These virulence factors are integral to the pathogenesis of *C.*
78 *neoformans* and as such, have been well-studied. However, *C. neoformans* utilizes additional
79 virulence factors which remain significantly understudied or completely unknown. For example,
80 we previously identified *PDR6* (also known as *AFR3*), a novel ATP-binding cassette (ABC)
81 transporter of the pleiotropic drug resistance (PDR) class, and showed that it had a role in various
82 cryptococcal virulence facets (12, 13). Present only in plants and fungi, PDR transporters
83 hydrolyze ATP to transport substrates across biological membranes and have been primarily
84 implicated in antifungal resistance (14, 15). Indeed, deletion of *PDR6* (*pdr6*Δ) results in hyper-
85 susceptibility to the azole-class of antifungals, but also showed *in vitro* and *in vivo* defects in
86 virulence. Thus, the role of *PDR6* in fungal pathogenesis and modulating the host immune
87 response warranted further investigation.

88 During microbial infections, the host's immune system is tasked with mounting an
89 appropriate and balanced immune response that will clear the infection while hopefully limiting
90 tissue damage (16). An exaggerated Th1, or pro-inflammatory, response will likely clear a
91 microbial infection but also result in excessive cellular and tissue damage. Opposingly, an
92 inappropriate Th2, or anti-inflammatory, response will certainly limit host damage but allow for
93 uncontrolled microbial proliferation and dissemination. Many pathogens take advantage of this
94 dichotomy to promote their infection. For example, early in HIV infection, this virus promotes the
95 secretion of pro-inflammatory cytokines IFN-γ and TNF-α, generating a strong Th1 response that
96 is permissive to viral replication (17, 18). In the context of *C. neoformans* infections, the fungus
97 promotes an anti-inflammatory Th2 response that allows for intracellular survival and increased

98 replication and dissemination, ultimately resulting in patient mortality (19, 20). It is evident,
99 however, that between these two immune response extremes, there is a whole spectrum of
100 responses to microbial infections, making this topic extremely complex but also an important
101 target for therapeutics. Hence, increased understanding of the immune response against
102 *Cryptococcus* can inform future therapeutic strategies where the immune response could be
103 modulated to benefit the host.

104 Our previous work characterized a novel PDR transporter with important roles in
105 cryptococcal biology and presented evidence consistent with *PDR6* being a new fungal virulence
106 factor (12). Here, we study the role of *PDR6* in the establishment and progression of disease using
107 a murine inhalation model of cryptococcosis. We show that a lower inoculum and significantly
108 decreased *pdr6*Δ fungal burdens are still not sufficient to clear infection by this mutant. Instead,
109 the survival studies and histological analysis suggests that the *pdr6*Δ mutant elicits an altered
110 host immune response characterized by significant increases in pro-inflammatory
111 cytokines/chemokines and innate immune cells. We treated the *pdr6*Δ-infected mice with a
112 corticosteroid and significantly extended their survival despite little to no change in fungal
113 burden. This dysregulated immune response might be a consequence of fungal surface
114 alterations that expose antigenic and immunogenic components that normally would be hidden
115 from the immune system. Collectively, this study furthers our understanding of cryptococcal
116 pathogenesis, highlights the clinical importance of the host immune response in controlling
117 fungal infections, while also providing novel functions and insights of fungal PDR-type
118 transporters in the context of disease progression.
119

120 **RESULTS**

121 ***pdr6*Δ-infected mice succumb to infection despite decreased inoculum and fungal burden.** In
122 our previous study we determined that *PDR6* was required for complete cryptococcal virulence
123 as mice infected with the *pdr6*Δ mutant lived significantly longer and had decreased fungal
124 burdens when compared to their H99-infected littermates (12). Consistently, this finding was
125 recapitulated by *Oliveira et al.* using the *Galleria mellonella* invertebrate infection model (13).
126 Notably, the *pdr6*Δ-infected animals displayed altered symptomatology compared to their H99-
127 infected littermates. Specifically, at endpoint, the WT-infected mice displayed altered behavior
128 associated with neurological deficiencies, traditional of cryptococcal meningitis; in contrast, the
129 *pdr6*Δ-infected mice exhibited respiratory symptoms characterized by rapid and labored
130 breathing, suggestive of pneumonia. We hypothesized that the altered symptomatology could
131 be explained, in part, by differences in the establishment and progression of disease. Previously,
132 fungal burdens were only quantified at time of death (TOD), potentially overlooking differences
133 earlier on in the infection. To obtain a comprehensive view of the infection over time, we
134 inoculated mice with 5 x 10^4 cells of H99 or *pdr6*Δ strains, and quantified fungal burden every
135 seven days over the course of the infection (Fig. 1A). Interestingly, we found that at 7 days post
136 infection (dpi) there were no differences in the fungal burdens between the H99 and *pdr6*Δ-
137 infected animals in all organs tested, suggesting that the strains established infection similarly.
138 Following this initial establishment, however, at 14 dpi there was a significant decrease in fungal
139 burden for the *pdr6*Δ strain compared to the WT. At 17 dpi, the H99-infected mice succumbed to
140 the infection with lung, brain, and spleen burdens of 3.7 x 10^8, 1.9 x 10^6, and 1.3 x 10^4 CFU while
141 the *pdr6*Δ-infected mice CFUs were 3.6 x 10^7, 2.3 x 10^4, and 677, respectively. Between 14 and

142 28 dpi, the fungal burden of the *pdr6*Δ-infected animals remains relatively constant in the brain
143 and spleen, with a gradual, although small, increase in the lungs. Then, after 28 dpi, there are
144 gradual increases in all organs with final CFU counts of 5.5 x 10^7, 1.1 x 10^5, and 1.5 x 10^3 in the
145 lungs, brain, and spleen, respectively. The differences in CFUs highlight key differences between
146 H99 and *pdr6*Δ disease progression and suggests a potential role of the adaptive immune
147 response given the changes at 14 dpi.

148 Experimentally, the mice in our previous studies were inoculated with 5 x 10^4 cells, a
149 common inoculum for the murine inhalation model of cryptococcosis. Given the *in vitro* defects
150 of the *pdr6*Δ strain (12), and the fact that initially, the mice were able to control the infection
151 (Fig. 1A), we hypothesized that by lowering the fungal inoculum, the survival of the *pdr6*Δ-
152 infected mice would be extended with a potential for complete clearance of the infection. To
153 assess this, we decreased the initial inoculum 10-fold and infected mice with 5 x 10^3 cells and
154 monitored survival (Fig. 1B). The H99-infected mice had a mean survival of 21 days and the *pdr6*Δ-
155 infected mice displayed a mean survival of 36 days, similar to our studies with 10-fold higher
156 inoculum. Quantification of the fungal burden showed similar CFUs in all organs between the
157 animals infected with low and high WT inoculum (Fig. 1C compared to 1A); however, despite
158 having similar lungs CFUs, the animals infected with low *pdr6*Δ inoculum had lower brain and
159 spleen CFUs at TOD relative to the higher inoculum (Fig. 1C compared to 1A). Evidently, using a
160 lower inoculum did not change the trend we have seen before: the *pdr6*Δ-infected mice still
161 survive longer with significant decreases in fungal burden across all organs. However, notably, in
162 the *pdr6*Δ-infected mice the lower inoculum results in lower overall organ burdens, with less

163 dissemination, yet the *pdr6*Δ-infected mice still succumbed to the infection with the same
164 dynamics as when using a higher inoculum (35-38 days; Fig. 1B).
165
166 **Infection with *pdr6*Δ results in increased tissue damage.** Despite initially colonizing the
167 pulmonary environment, the *Cryptococcus*-associated fatal pathology occurs in the brain due to
168 the meningoencephalitis (21, 22). The altered symptomatology coupled with the differential
169 disease progression suggests that the *pdr6*Δ strain likely affects the host immune response.
170 Furthermore, when performing the previous fungal burden experiments, we observed significant
171 phenotypic differences in lung sizes in H99 v. *pdr6*Δ-infected mice (Fig. 2). To qualitatively assess
172 any potential differences at the cellular and tissue level, we harvested the lungs of mock, H99,
173 and *pdr6*Δ-infected mice, stained with hematoxylin and eosin (H&E), and assessed tissue damage
174 (Fig. 2 and Table 1). At 14 dpi, the gross anatomical images clearly show increased size and
175 inflammation of the H99-infected lungs when compared to the *pdr6*Δ-infected. Additionally, the
176 10X and 40X images display deterioration of the lung parenchyma and infiltration of *C.*
177 *neoformans* which is not observed in the *pdr6*Δ-infected lungs (Fig. 2A). At 35 dpi, the *pdr6*Δ-
178 infected lungs are severely inflamed, infiltrated with yeast, and characterized by the presence of
179 many inflammatory immune cells in the peri-bronchial and perivascular space (Fig. 2B). Table 1
180 provides a quantitative summary comparing the H99 and *pdr6*Δ-infected pulmonary tissue over
181 time. Consistent with our observations in the fungal burden experiments, there were little to no
182 differences at 7 dpi. However, at 14 dpi the *pdr6*Δ-infected lung contains the yeast in granuloma-
183 like regions and have 30% less *C. neoformans* than the WT-infected tissues. Furthermore, an
184 increase in lymphocytes is observed in the *pdr6*Δ-infected lungs relative to WT (105 to 26,

185 respectively; Table 1). Finally, as the *pdr6*Δ-infected mice approach TOD, the fungal infiltration,
186 inflammation, and number of inflammatory immune cells in the lung tissue all increase to levels
187 well above those observed in the WT-infected animals at TOD. Altogether, these findings suggest
188 that the *pdr6*Δ strain elicits a differential immune response in the pulmonary environment thus
189 affecting disease progression and symptomatology.
190
191 **Fluconazole treatment improves fungal burden but not outcome in *pdr6*Δ-infected mice.**
192 Currently, there a very few antifungal drugs available to treat cryptococcal infections and the
193 compounds that are available are either not effective, extremely expensive, or associated with
194 deleterious side effects (23). Fluconazole (FLC), a fungistatic azole class antifungal, is the mainstay
195 treatment option in low-resource regions where cryptococcal infections are endemic.
196 Mechanistically, FLC inhibits lanosterol 14α-demethylase, an enzyme in the ergosterol
197 biosynthesis pathway encoded by *ERG11* (24). In our previous study, we showed that the deletion
198 of *PDR6* increased the susceptibility of *C. neoformans* to azole class antifungals including FLC (12).
199 Given this phenotype, we hypothesized that treatment of *C. neoformans pdr6*Δ-infected mice
200 with FLC would result in total clearance of the infection, preventing the lethal immune pathology.
201 To test this, mice infected with either the WT or *pdr6*Δ strains, or mock infected, were treated
202 daily (starting 1 dpi) with either a low (8 mg/kg) or high dose (16 mg/kg) of FLC and monitored
203 for survival (Fig. 3A). The FLC treatment significantly extended survival in both the H99 and *pdr6*Δ-
204 infected animals compared to the untreated controls. Unfortunately, survival was extended to
205 the same extent for both groups. Numerically, the mean survival for the untreated H99-infected
206 mice was 17 days and the low and high doses extended survival 4.5 and 6 days, respectively.

207 Similarly, the mean survival for the untreated *pdr6*Δ-infected mice was 34 days and the low and
208 high doses extended survival 5 and 7 days, respectively. Surprisingly, although the survival was
209 similarly extended between strains, quantification of the fungal burden revealed significant
210 differences (Fig. 3B-G). At 14 dpi, both doses of the FLC treatment significantly decreased the
211 fungal burden in the lungs, brain, and spleen only in the *pdr6*Δ-infected mice (Fig. 3B-D). Similarly,
212 at TOD, the daily FLC treatment continued to lower the fungal burden of the *pdr6*Δ-infected mice
213 even more across all three organs, with several mice where the brain and spleen CFU counts were
214 at the limit of detection (LOD) (Fig. 3E-G). Not surprisingly, neither of the FLC doses had a
215 significant effect on WT-infected mice. This observation is interesting because despite
216 significantly decreasing the fungal burden with the FLC treatment, the *pdr6*Δ-infected animals
217 were still succumbing to the infection.

218 To understand how the FLC treatment was affecting the pulmonary environment, we
219 prepared slides and performed qualitative histological analysis at TOD for both WT and *pdr6*Δ-
220 infected mice (Fig. 4 and Table 2). The H99-infected lungs at 14 dpi treated with FLC displayed
221 similar features to the previously pictured H99 untreated lungs, namely a high percentage of
222 fungal infiltration and tissue breakdown. In contrast, the *pdr6*Δ-infected lungs at 35 dpi treated
223 with FLC appear to have the infection controlled in granuloma-like regions (Fig. 4, inset 2) with
224 widespread immune cell infiltration (Fig. 4, inset 1). Interestingly, despite reduced pulmonary
225 CFUs (Fig. 3 and Table 2) and decreased inflammation (Fig. 4 and Table 2), the *pdr6*Δ-infected
226 mice were still succumbing to the infection. Together, these data suggest that the mice infected
227 with the *pdr6*Δ-strain are not necessarily dying directly because of the *C. neoformans* infection,
228 but rather indirectly because of an inappropriate host immune response.

229

230 ***C. neoformans pdr6*Δ strain elicits a strong pro-inflammatory immune response.** During
231 microbial infections, the host's immune response ultimately determines the clinical outcome
232 (25). Ideally, a balanced Th1 pro-inflammatory and Th2 anti-inflammatory immune response will
233 allow for microbial clearance and subsequent tissue repair. Previous studies have determined
234 that *C. neoformans* skews the immune response towards a permissive anti-inflammatory Th2
235 response, thus benefiting the yeast and allowing for fungal replication and subsequent
236 dissemination (26). Given our previous observations, we hypothesize that the *pdr6*Δ strain is
237 instead generating a strong pro-inflammatory immune response that is able to control the
238 infection initially, but also damaging large areas of pulmonary tissue. To assess this, we quantified
239 the secreted cytokines and chemokines profile in the lungs and brains of H99 and *pdr6*Δ-infected
240 mice at their respective TODs (Fig. 5). Interestingly, we found that several of the pro-
241 inflammatory cytokines are significantly upregulated in the *pdr6*Δ-infected lungs relative to WT
242 (Fig. 5A). Specifically, the production of IL-1α, IL-1β, and MIP-1β (macrophage inflammatory
243 protein 1β) is increased 13-fold, 23-fold, and 29-fold respectively, when compared to the lungs
244 of the H99-infected mice. Additionally, the expression of several anti-inflammatory cytokines like
245 IL-9, IL-13, and IL-33 are lower in the *pdr6*Δ-infected mice relative to WT. A similar trend was
246 observed in the brain although not to the same extent as that observed in the pulmonary tissues
247 (Fig. 5B). Specifically, the pro-inflammatory cytokines/chemokines IL-1β, KC (keratinocyte
248 chemoattractant), and TNF-α (tumor necrosis factor α) are all highly expressed when normalized
249 to the H99-infected brain, and the anti-inflammatory cytokines IL-4 and IL-9 display decreased
250 expression in the brain when compared to WT. The decreased capacity of the *pdr6*Δ mutant to

251 survive in host phagocytes and disseminate coupled with the immune-privileged status of the
252 CNS may explain the weakened expression of inflammatory cytokines in the brain. During a
253 typical cryptococcal infection, the expression of anti-inflammatory cytokines/chemokines are
254 increased thus generating a Th2 response, however, in the context of an infection with the *pdr6*Δ
255 strain, the secretion of pro-inflammatory cytokines/chemokines is significantly increased
256 resulting in a damaging Th1 immune response.
257
258 **Corticosteroid treatment extends survival in *pdr6*Δ-infected mice.** Clinically, corticosteroids like
259 dexamethasone are prescribed to downregulate the immune system. Mechanistically, these anti-
260 inflammatory drugs function by suppressing the migration of neutrophils and decreasing
261 lymphocyte colony proliferation (27). The potential of dexamethasone as a treatment strategy
262 during cryptococcal infection was investigated in a clinical trial but was prematurely concluded
263 because of adverse effects and increased mortality (28, 29); however, corticosteroids have been
264 used successfully to treat CME-associated inflammatory disorders such as postinfectious
265 inflammatory response syndrome and immune reconstitution inflammatory syndrome (21).
266 Given the robust pro-inflammatory immune response observed in the *pdr6*Δ-infected mice, we
267 hypothesized dexamethasone treatment would dampen or knock down the aggressive Th1
268 response resulting in fungal clearance and improved survival. Experimentally, we infected mice
269 with either the H99 or *pdr6*Δ strain, or mock infected, and treated them daily (starting at 1 dpi)
270 with either 0.3 mg/kg dexamethasone or a dexamethasone and 16 mg/kg FLC combination and
271 assessed survival (Fig. 6A). The H99-infected mice that received the dexamethasone treatment
272 displayed a significant reduction in survival (mean survival of 13 days vs 17 days) when compared

273 to the untreated H99 control, while the combo therapy restored survival to that of the untreated
274 H99-infected group (mean survival of 16 days vs 17 days). This result corroborates the
275 corticosteroid finding reported in the human clinical trial. In terms of the *pdr6*Δ-infected mice,
276 both the dexamethasone alone and in combination with FLC significantly extended survival.
277 Numerically, the mean survival of the untreated *pdr6*Δ-infected control group was 34 days and
278 was extended to 55 and 58 days in the dexamethasone and combination treated groups,
279 respectively. The survival studies were stopped after 60 dpi because the remaining mice,
280 including the mock-infected receiving the daily dexamethasone treatment (not shown),
281 appeared sick despite not meeting endpoint criteria. We concluded that after two months of
282 daily corticosteroid injections the immune systems of the mice had been ablated resulting in their
283 poor appearances. Despite the dexamethasone treatment extending survival in the *pdr6*Δ-
284 infected animals, the fungal burdens were differentially affected over the course of the
285 experiment (Fig. 6B-G). Specifically, at 14 dpi the addition of dexamethasone significantly
286 decreased the fungal burden in the lungs in both the H99 and *pdr6*Δ-infected mice and little to
287 no changes were observed in either strain in the brain or spleen CFUs (Fig. 6B-D). At TOD the
288 dexamethasone treatment in the *pdr6*Δ-infected animals significantly increased the lung CFUs
289 and the combination therapy returned it to levels comparable to the untreated *pdr6*Δ-infected
290 control (Fig. 6E). Although not statistically significant, a similar trend was observed in the brain
291 and spleen of the *pdr6*Δ-infected mice (Fig. 6F & G). These effects were not seen in the WT-
292 infected mice. The dynamic changes in fungal burdens in the lungs of the dexamethasone and
293 combination treated *pdr6*Δ-infected mice can be explained by the absence or lack of
294 inflammatory immune cells to control the infection and the addition of FLC lowers the CFU as the

295 fungistatic nature of the antifungal is unable to clear the initial infection. Collectively, these data
296 further confirm and highlight the altered disease progression elicited by the *pdr6*Δ mutant and
297 more importantly demonstrate the positive clinical outcome associated with controlling the
298 inappropriate pro-inflammatory immune response.
299
300 **Combination dexamethasone and fluconazole treatment reduces pulmonary tissue damage in**
301 ***pdr6*Δ-infected animals.** Based on our previous results, it is evident that the addition of the
302 corticosteroid is benefiting the *pdr6*Δ-infected mice by significantly extending survival.
303 Histological analysis of the lung tissue at TOD for both WT and *pdr6*Δ-infected mice was
304 performed to visualize changes in fungal infiltration, tissue inflammation, and immune cell
305 recruitment (Fig. 7 and Table 3). Visually, the treatment with dexamethasone had a profound
306 effect given the qualitative reduction in inflammatory cells across all conditions. The lungs of the
307 H99-infected mice that received dexamethasone are not as inflamed as what was observed on
308 our previous slides but the destruction of the lung tissue is devastating (Fig. 7A). Clearly the lack
309 of immune cells allowed for the uncontrolled proliferation of *C. neoformans* resulting in increased
310 damage of the pulmonary tissue. Similarly, the dexamethasone treated lungs of the *pdr6*Δ-
311 infected display intense fungal proliferation but there is qualitatively less damage when
312 compared to the H99-infected animals (Fig. 7B and Table 3). The combination dexamethasone
313 and FLC treatment reduced the fungal infiltration in both the H99 and *pdr6*Δ-infected mice when
314 compared to the dexamethasone alone (Fig. 8 and Table 4). In fact, despite the presence of some
315 yeast, the *pdr6*Δ-infected lung tissue appears relatively healthy with little to no damage and

316 inflammation suggesting that another mechanism may be responsible for the mice reaching
317 endpoint (Fig. 8B and Table 4).
318
319 ***pdr6*Δ-infected mice display an increase in innate immune cells populations.** During microbial
320 infections, the cells of the innate immune system represent the first line of defense which is
321 followed by the activation and recruitment of the adaptive immune response (30). In a *C.*
322 *neoformans* infection, lung macrophages represent the innate population primarily responsible
323 for initial clearance, although some recent literature suggests neutrophils also play an important
324 role (31-33). However, CME is an AIDS-defining disease, and low $CD4^+$ T-cell counts is a major
325 susceptibility for CME, indicating that the adaptive immune response also plays an important role
326 controlling cryptococcal infections (34). Provided the altered immune response to the *pdr6*Δ
327 strain, we expected alterations to both the quantity and the composition of innate and adaptive
328 inflammatory immune cells. To test this, we harvested leukocytes from the lungs of H99 and
329 *pdr6*Δ-infected mice at 14 dpi (close to TOD of WT-infected mice) and at 35 dpi (close to TOD of
330 *pdr6*Δ-infected mice) and quantified the different populations using flow cytometry (Fig. 9).
331 Quantification of the total innate immune cell populations at 14 dpi showed that the FLC,
332 dexamethasone, and combination treatments led to a significant decrease in the *pdr6*Δ-infected
333 animals whereas there were no significant changes in the H99-infected mice (Fig. 9A). A similar
334 trend was observed when compared as a percentage of $CD45^+$ cells. Interestingly, a significant
335 increase in neutrophils and macrophages was seen in the combination-treated *pdr6*Δ-infected
336 mice (Fig. 9B). At this time (14 dpi), quantification of the total adaptive immune cells showed a
337 marked increase in the *pdr6*Δ-infected animals when compared their H99-infected counterparts,

338 although only the $CD8^+$ T-cells were statistically significant (Fig. 9C, untreated bars). Furthermore,
339 all treatments decrease the number of adaptive immune cells in the *pdr6*Δ-infected animals
340 relative to the WT, specially the $CD8^+$ T-cells (Fig. 9C, FLC, Dexa, and +Dexa +FLC bars). The same
341 trend is observed when compared as percentage of CD45+ cells (Fig. 9D). At 35 dpi there are
342 some minor differences in the adaptive immune cell populations when comparing the treated
343 groups (Fig. 9G & H) but the interesting finding is observed in the innate immune cell populations
344 (Fig. 9E & F). Specifically, a significant increase in macrophages is observed in the *pdr6*Δ-infected
345 mice when compared to the H99-infected (Fig. 9E & F, untreated bars). Furthermore, the
346 dexamethasone treatment in the *pdr6*Δ-infected animals significantly decreases the number of
347 macrophages which is replaced by a significant increase in the number of neutrophils (Fig. 9E &
348 F, Dexa bars). It appears that in the absence of Pdr6, the neutrophil response is more robust and
349 sustained than the macrophage response, whereas is the opposite in the WT-infected mice.
350 Collectively, these results showed that infection with the *pdr6*Δ strain results in the increased
351 recruitment of adaptive immune cells early on during the infection while an increase in innate
352 immune cells, specifically macrophages, was observed in the later stages of the disease. This
353 further explains the strong pro-inflammatory response, altered disease progression, and
354 differential symptomatology specific to the *pdr6*Δ strain.
355
356 ***C. neoformans pdr6Δ* strain exhibits increased PAMP exposure.** Up to this point we have shown
357 that the infection of our mouse model with the *C. neoformans pdr6*Δ strain results in the
358 recruitment of more inflammatory immune cells leading to increased pulmonary damage and
359 mortality. Further support was provided in the dexamethasone treatment experiments, where

360 dampening the immune response significantly extended survival in the *pdr6*Δ-infected animals.
361 Experimentally, we have studied the host response to this cryptococcal mutant but the question
362 that remains is how is this mutant modulating the immune system and generating a robust Th1
363 response? In our previous work, we showed that *PDR6* encodes an atypical transporter localized
364 to the endoplasmic reticulum (ER) and plasma membrane (PM) involved in ergosterol trafficking
365 (12). Others have suggested a direct relationship between altered ergosterol levels and host
366 immune responses (35, 36) as well as altered surface composition due to defects in PM fluidity
367 and lipid rafts (37, 38) We hypothesized that in deleting this transport protein there would be
368 less ergosterol in the PM, potentially resulting in downstream alterations to the cryptococcal
369 surface and an increase in exposed immunogenic components. To assess this, we grew H99 and
370 *pdr6*Δ cells in YPD, stained with fluorescent dyes that recognize and bind to fungal cell wall
371 components, and visualized the cells using microscopy. Under this condition, we did not observe
372 any difference between the H99 and *pdr6*Δ stained cells (data not shown). However, previous
373 studies have reported a correlation between growth conditions and the architecture of the fungal
374 cell wall (39). This led us to repeat the experiment with cells grown under host-like conditions
375 (DMEM at 37°C + 5% CO_2) (Fig. 10A). Under these conditions, the *pdr6*Δ strain displayed increase
376 staining with calcofluor white (CFW) and concanavalin A (ConA) suggestive of increased exposure
377 of chitin and mannoproteins, respectively. Similarly, there was an increase in binding of the β-
378 (1,3)-glucan antibody suggestive of more exposed β-glucans in the *pdr6*Δ mutant (Fig. 10A).
379 Quantification of CFW, ConA, and eosin Y (EoY), which binds/stains chitosan, using flow
380 cytometry revealed a significant increase in the binding of all the stains in the *pdr6*Δ strain when
381 compared to the WT (Fig. 10B). The *cap59*Δ mutant, deficient in polysaccharide capsule synthesis

382 and thus with increased exposure of its cell wall, was used as a positive control. Having previously
383 shown that the pdr6 mutant has no defect in capsule induction, we hypothesized that alterations
384 in the capsular architecture could justify the increase in exposed cryptococcal PAMPs. To assess
385 this, we used several anti-polysaccharide capsule antibodies to stain the capsules of H99, *pdr6Δ*,
386 and *cap59*Δ cells (Fig. 10C). A significant increase in staining and penetration of the antibody was
387 observed in the *pdr6*Δ mutant when using the mAb 302. This antibody only recognizes and binds
388 acetylated GXM (40) and suggests that the integrity and/or porousness of the polysaccharide
389 capsule in the *pdr6*Δ strain is altered when compared to the structurally-sound WT capsule.
390 Altogether, these findings suggest that the deletion of *PDR6* disrupts the cryptococcal cell wall
391 composition and the capsule density (since it is induced to normal size in the *pdr6*Δ mutant),
392 allowing for increased exposure of fungal PAMPs, namely chitin, mannoproteins, and β-glucans.
393 This observed increase in PAMP exposure in the *pdr6*Δ strain can mechanistically explain the
394 increased pro-inflammatory response by the host immune system.
395

396 **DISCUSSION**

397 Fungal PDR transporters are primarily considered virulence factors because of their role in
398 antifungal resistance. For example, the overexpression of *AFR1* in *C. neoformans* and *CDR1* in *C.*
399 *albicans* clinical strains increase their resistance to many of the azole class antifungals and
400 complicates the treatment strategy (41, 42). Structurally, these two proteins (and all other well-
401 characterized fungal PDR transporters) are 'full-length' consisting of two nucleotide-binding
402 domains (NBDs) and two transmembrane domains (TMDs), which is required for a functional
403 fungal PDR protein (15, 43). Here, we continue the characterization of *C. neoformans PDR6*, an

404 atypical and novel 'half-size' PDR transporter since it only possesses one NBD and one TMD.
405 Given the asymmetrical nature of PDR transporters and the conserved 'degenerated' sequence
406 in one of the NBDs, it is unlikely that Pdr6 homo-dimerizes and instead hetero-dimerizes with
407 another half-size PDR protein present in the cryptococcal genome (of which there are two more)
408 to form a functional transporter (14). An interesting future direction includes the identification
409 and subsequent deletion of Pdr6's binding partner which should generate phenotypes similar to
410 those observed in the *pdr6*Δ strain. Nevertheless, we found that in addition to azole resistance,
411 *PDR6* modulates the host immune response, a phenotype that may be unique to 'half-size' PDR
412 transporters (12).

413 The *pdr6*Δ-dependent alterations in survival, fungal burden, and symptoms all suggested
414 a differential host response. Specifically, the fact that the significant decrease in fungal burden
415 across all organs coupled with the lower inoculum still resulted in mortality showed that the mice
416 infected with the *pdr6*Δ mutant were not succumbing because of the fungus, but because of an
417 inappropriate and damaging immune response. Consistently, the treatment of the *pdr6*Δ-
418 infected mice with FLC decreased the fungal burden in all organs, and in some to the limit of
419 detection, and yet the mice still died, implicating the immune system. Furthermore, the
420 divergence in symptoms between the WT and *pdr6*Δ-infected animals at TOD was clinically
421 relevant. Although the *pdr6*Δ-infected mice displayed a pneumonia-like symptomatology rather
422 than the expected neurological symptoms, they still had CFUs in the brain so CME cannot be ruled
423 out; however, we think that it was below the threshold to trigger the symptoms and the
424 neurological deficiencies characteristic of CME. The histological analysis, immune cell
425 quantification, and cytokine/chemokine expression profiles all showed an aggressive lung pro-

426 inflammatory immune response against the *pdr6*Δ mutant, while the response in the brain was
427 more muted, substantiating our claim. After understanding that the *pdr6*Δ-infected mice were
428 dying because of a sustained Th1 immune response, we expected the corticosteroid treatment
429 experiment would result in total clearance of the infection. The dosages of the dexamethasone
430 and FLC were based off clinical reports and we purposefully used the lower dexamethasone dose
431 given the extended length of the proposed experiment (28). We show that the addition of
432 dexamethasone significantly extended the survival of the *pdr6*Δ-infected mice although the
433 infection was not cleared even with the addition of FLC. Notably, the combo treatment reduced
434 both inflammation and fungal burden in the lungs and restored tissue architecture almost to
435 normal, but the outcome was not significantly different. Optimizing the timing of the
436 dexamethasone treatments, such that it is not administered for the entirety of the experiment,
437 or the doses are tapered after an initial pulse, warrants further investigation and represents a
438 future direction. Since corticosteroids are immunosuppressive, and the i.p. injection of
439 dexamethasone will dampen the immune response in the whole body, it is possible that while
440 eliminating the tissue damage in the lungs, the treatment also inhibits the clearance of the yeast
441 in other organs (most likely kidneys, liver, or heart), explaining the eventual death after extending
442 survival for more than three weeks. In that sense, if the dexamethasone could be targeted to
443 specifically affect the lung tissue, as with the use of an inhaler, we would expect a better
444 outcome.

445 The *in vivo* experimentation allowed us to comprehend what was occurring within the
446 host, but why was this specifically occurring with the *pdr6*Δ strain? Our data showing that the
447 *pdr6*Δ mutant displays increased PAMP exposure is a reasonable explanation for the pro-

448 inflammatory response. However, it may not be the only reason as the acapsular *cap59*Δ mutant
449 also exhibits increased PAMP exposure and it is avirulent in the same mouse model. Furthermore,
450 we previously showed that conditioned media (CM) from *pdr6*Δ cultures modulates the
451 phagocytosis of *C. neoformans* by macrophages, whereas the CM from *cap59*Δ or other PDR
452 transporter mutants had little to no effect (12), suggestive of an immunomodulatory Pdr6-
453 dependent secreted factor. Nevertheless, all these data identify and support Pdr6 as a potential
454 therapeutic target. Anticryptococcal treatments are limited by toxicity, costs, and rising microbial
455 resistance, but FLC, despite being sub-optimal, still is the antifungal of choice in many regions of
456 the world because it is cheap, relatively less toxic, and broad spectrum. Since the deletion of
457 *PDR6* results in hypersensitivity to FLC, the design and synthesis of a novel compound that targets
458 Pdr6, coupled with FLC and/or a corticosteroid, may have clinical potential. Alternatively, several
459 groups in the cryptococcal and immunology fields have tried to identify potential vaccine
460 candidates against this fungus (44). Collectively, these preliminary vaccines, elicit a pro-
461 inflammatory response allowing for protection against subsequent challenges (45-47). However,
462 this is hampered because the immune mechanisms that elicit a protective immune response are
463 not known yet. Thus, the knowledge generated in this study has potential to help inform
464 cryptococcal vaccine development by providing novel insights into what constitutes a deleterious
465 pro-inflammatory response against *C. neoformans* infection.

466 Finally, the complexities of PDR half-size transporters still remain unknown. It is
467 understood that these proteins are promiscuous and transport a diverse array of substrates, and
468 coupled with the expanded repertoire of PDR genes in *Cryptococcus*, it is not surprising to find
469 roles other than traditional efflux pumps and subsequent resistance to xenobiotics. *PDR6* has

470 also been implicated in aging and replicative life span (13), and most recently, *PDR9*, a full-length
471 PDR gene in the same clade as *AFR1*, was found to play a role in CO_2 tolerance via an unknown
472 mechanism that may involve phospholipid flipping (48). Hence, *PDR6* may act through multiple
473 direct and indirect mechanisms to modulate the inflammatory host response, such as by
474 secreting immunomodulatory molecules, aiding in maintaining the correct PM fluidity by
475 regulating ergosterol transport, and preventing exposure of surface PAMPs by supporting correct
476 cell wall and/or capsule architecture. All of these functions could be mediated by Pdr6-
477 dependent metabolites, lipids, or proteins, supporting future studies in these areas such as
478 comparative metabolomics of WT and *pdr6*Δ CM.

479 In conclusion, we have further characterized a novel virulence factor in *C. neoformans* by
480 studying the role of *PDR6* in a mouse model of cryptococcosis and examining the altered immune
481 response. Mice infected with the *pdr6*Δ strain still perished despite a lower initial inoculum, lower
482 organ burdens over the course of infection, significantly decreased fungal CFUs when treated
483 with FLC, and muting of an overexuberant inflammatory response when treated with
484 dexamethasone. *PDR6* is not necessarily involved in the establishment of disease, as there was
485 no difference in CFUs 7 dpi relative to WT, but it is critical in the progression of cryptococcosis as
486 mice succumbed to a fulminant pneumonia rather than CME. This is because in its absence, there
487 is increased exposure of immunomodulatory chitin, chitosan, mannoproteins, and β-glucans,
488 contributing to the secretion of pro-inflammatory cytokines and chemokines which increase the
489 number of macrophages and other inflammatory immune cells in the lungs, containing the
490 infection but causing devasting tissue damage and inflammation. Elucidating the role of *PDR6* in
491 the context of infection improves our understanding of cryptococcal pathogenesis while also

492 informing potential clinically relevant therapeutic studies such as the search for novel drug
493 targets or the development of a vaccine. More broadly, this study expands the field of fungal PDR
494 transporters and given the conserved nature of these proteins, these findings may be applicable
495 to other fungal pathogens.
496

497 **MATERIALS & METHODS**

498 **Strains, media, and growth conditions.**

499 All *C. neoformans* strains used in this study were in the serotype A H99α background. All fungal
500 strains were maintained at -80ºC and grown at 30ºC on yeast peptone dextrose (YPD) with
501 antibiotics (NAT or G418) as appropriate.

502 **Murine survival studies**

503 *In vivo* fungal virulence was tested in our murine inhalation model of cryptococcosis (12, 49-51).
504 Briefly, 5- to 6-week-old female A/J inbred mice (The Jackson Laboratories) were anesthetized
505 with a ketamine rodent cocktail delivered i.p. and intranasally inoculated, unless otherwise
506 stated, with 5.0 x 10^4 cryptococcal cells in 40 μL of sterile PBS. Animals were closely monitored
507 and humanely euthanized if they lost >20% weight relative to peak weight, or at predetermined
508 timepoints, or at the end of the experiment (maximum of 60 days).
509 For drug treatment studies, cryptococcal-infected mice were randomly assigned into treated or
510 non-treated control groups. Stock solutions of fluconazole (1.6 mg/mL), dexamethasone (0.03
511 mg/mL), and a fluconazole/dexamethasone combo were prepared in sterile PBS. The drug(s)
512 were administered intraperitoneally at doses of 16 mg/kg/day and 8 mg/kg/day for fluconazole
513 and 0.3 mg/kg/day for dexamethasone. In survival studies, treatment began 24 h after infection

514 and continued throughout the experiment until endpoint was reached. Statistically significant
515 differences between survival curves were determined by log rank Mantel-Cox test (GraphPad
516 Prism).

517 **Fungal Burden Quantification**

518 Infected mice were humanely euthanized at predetermined time points or TOD by isoflurane
519 overdose followed by cervical dislocation, and lungs, brain, and spleens were harvested. Tissues
520 were homogenized in 5 mL of sterile PBS, diluted, and plated on YPD agar medium supplemented
521 with ampicillin. CFUs were counted following incubation at 30°C for 48 h. Statistical significance
522 was determined using ANOVA Kruskal-Wallis test (GraphPad Prism).

523 **Histological analyses**

524 A/J female mice (The Jackson Laboratories) were infected via the intranasal route as described
525 above with 5 x 10^4 CFU of either WT (H99) or the *pdr6*Δ mutant strain. Mice were sacrificed as
526 predetermined time points (14, 35, 50 days post inoculation) by isoflurane overdose followed by
527 cervical dislocation. Lungs were perfused with sterile PBS and 10% neutralized formalin. Lungs
528 were subsequently paraffin embedded, sectioned, mounted, and stained with H&E by the
529 University of Notre Dame Histology Core facility. H&E-stained slides were imaged at 10X and 40X
530 using an inverted Zeiss microscope. Slides were scored in a blind manner by the resident
531 pathologist at the Harper Cancer Research Institute [W.J.K.].

532 **Cytokine Analyses**

533 A/J female mice from Jackson Laboratories were infected via the intranasal route with WT (H99)
534 or the *pdr6*Δ mutant strain as described above. Mice were euthanized at predetermined time
535 points by isoflurane overdose followed by cervical dislocation. Cytokine levels within the lung and

536 brain homogenates of infected mice were analyzed using the Proteome Profiler Mouse XL
537 Cytokine Array (R&D Systems Inc., Minneapolis, MN). The relative expression levels of 111 soluble
538 mouse proteins were determined following the manufacturer's protocol. Array membranes were
539 imaged using LI-COR Odyssey Infrared Imaging System and quantified using ImageStudio
540 software.

541 Cytokine/chemokine expression levels were further confirmed using the Bio-Plex Multi-Plex
542 Assay Kit (Bio-Rad Laboratories, Hercules, CA). Supernatants from organ homogenates were
543 used to determine presence of 22 proteins including eotaxin, G-CSF, GM-CSF, IFN-γ, IL-1α, IL-1β,
544 IL-2, IL-3, IL-4, IL-6, IL-9, IL-10, IL-12 (p40), IL-12 (p70), IL-13, IL-17A, KC, MCP-1, MCP-1α, MIP-1β,
545 RANTES, and TNF-α.

546 **Pulmonary leukocyte isolation and flow cytometric analysis**

547 H99 and *pdr6*Δ-infected mice were euthanized at predetermined time points and TOD by
548 isoflurane overdose followed by cervical dislocation. Lungs of infected mice were excised and
549 digested enzymatically at 37°C for 60 min in 10 mL of digest buffer (0.34 U/mL Liberase™ (Roche)
550 and 100 ug/mL DNaseI (ThermoFisher)) in 1X DPBS. After 60 min, digestion was arrested with 1X
551 DPBS supplemented with 2% FBS and 0.2 um EDTA. The cell suspension was washed and passed
552 through 40-μm cell strainers.

553 The single cell suspensions were stained with a live/dead far red viability dye (Invitrogen),
554 washed, and incubated on ice for 20 min with purified anti-mouse CD16/CD32 antibodies
555 (BioLegend) to block Fc receptors. Following blocking, cells were incubated with fluorochrome-
556 conjugated antibodies to allow for multistaining for 45 min on ice. The innate panel consisted of
557 PE-Cy5 conjugated anti-CD45 (30-111), Brilliant Violet (BV) 650-conjugated anti-CD11b (M1/70),

558 Super Bright (SB) 780-conjugated anti-F4/80 (BM8), BV711-conjugated anti-Ly6G (1A8), PE-Cy7-
559 conjugated anti-Ly6C (HK1.4), PE-conjugated anti-SiglecF (1RNM44N), and APC-eFluor 780-
560 conjugated anti-CD11c (N418). The adaptive panel included PE-Cy5 conjugated anti-CD45 (30-
561 111), AF700-conjugated anti-CD3 (145-2C11), BV421-conjugated anti-CD4 (GK1.5), BV510-
562 conjugated anti-CD25 (PC61-5), PE-conjugated anti-CD8 (53-6.7), and AF488-conjugated anti-
563 FoxP3 (FJK-16s). Cells were washed and fixed with 2% formalin in FACS buffer. UltraComp eBeads
564 (Invitrogen) were stained with each respective fluorochrome-conjugated antibody and used to
565 determine and spillover/compensation calculations. Data was analyzed using FlowJo software.

566 **Cell wall and capsule stains**

567 Starter cultures were grown overnight in YPD, washed with DMEM, and 1 x 10^6 cells/mL were
568 added to 24-well tissue culture plates. Plates were incubated at 37°C + 5% CO2 for 48 h. The cells
569 were collected by centrifugation at 3,000 x g for 5 min. For staining, Calcofluor White (CFW),
570 Alexa Fluor 488-conjugated concanavalin A (ConA), β-(1,3)-glucan antibody 2GB (ab233743;
571 Abcam, USA), eosin Y (EoY), and the capsular antibody 302 were used. Cells were washed and
572 stained with CFW, ConA, β-(1,3)-glucan antibody, EoY, and Mab 302 at 100 µg/mL, 50 µg/mL, 20
573 µg/mL, 500 µg/mL, and 10 µg/mL, respectively. Cells were incubated with the stains for 30 min,
574 washed, fixed, and imaged at 100X using an inverted Zeiss microscope. Fluorescence of mAb 302
575 was calculated using Cell Profiler software. Flow cytometry data was acquired using a BD
576 LSRFortessa cytometer. The CFW signal was detected using a 405 nm laser and the ConA and EoY
577 signals were detected using a 488 nm laser. Flow cytometry data was analyzed with FlowJo
578 software.

579

580 **ACKNOWLEDGMENTS**

581 We acknowledge assistance and support on the murine studies from the University of Notre
582 Dame Freimann Life Science Center (FLSC). We give a special thanks to William J. Kaliney, M.D.,
583 pathologist from Harper Cancer Research Center, for assistance with histological analysis and
584 scoring. We acknowledge financial support from the Warren Center for Drug Discovery (pilot
585 grant) and NIH grant R21AI71742. We also thank members of the Santiago-Tirado lab for their
586 thoughtful comments and feedback on this work.

587

588 **REFERENCES**

589 1. Denning DW. 2024. Global incidence and mortality of severe fungal disease. Lancet Infect Dis
590 doi:10.1016/S1473-3099(23)00692-8.
591 2. Gaylord EA, Choy HL, Doering TL. 2020. Dangerous Liaisons: Interactions of Cryptococcus
592 neoformans with Host Phagocytes. Pathogens 9.
593 3. Stuckey PV, Santiago-Tirado FH. 2023. Fungal mechanisms of intracellular survival: what can we
594 learn from bacterial pathogens? Infect Immun 91:e0043422.
595 4. Rajasingham R, Govender NP, Jordan A, Loyse A, Shroufi A, Denning DW, Meya DB, Chiller TM,
596 Boulware DR. 2022. The global burden of HIV-associated cryptococcal infection in adults in
597 2020: a modelling analysis. Lancet Infect Dis doi:10.1016/S1473-3099(22)00499-6.
598 5. Santiago-Tirado FH, Doering TL. 2017. False friends: Phagocytes as Trojan horses in microbial
599 brain infections. PLoS Pathog 13:e1006680.
600 6. Denham ST, Brown JCS. 2018. Mechanisms of Pulmonary Escape and Dissemination by
601 Cryptococcus neoformans. J Fungi (Basel) 4.
602 7. Zaragoza O, Rodrigues ML, De Jesus M, Frases S, Dadachova E, Casadevall A. 2009. The capsule
603 of the fungal pathogen Cryptococcus neoformans. Adv Appl Microbiol 68:133-216.
604 8. Denham ST, Verma S, Reynolds RC, Worne CL, Daugherty JM, Lane TE, Brown JCS. 2018.
605 Regulated Release of Cryptococcal Polysaccharide Drives Virulence and Suppresses Immune Cell
606 Infiltration into the Central Nervous System. Infect Immun 86.
607 9. Alspaugh JA. 2015. Virulence mechanisms and Cryptococcus neoformans pathogenesis. Fungal
608 Genet Biol 78:55-8.
609 10. Pacelli C, Bryan RA, Onofri S, Selbmann L, Shuryak I, Dadachova E. 2017. Melanin is effective in
610 protecting fast and slow growing fungi from various types of ionizing radiation. Environ
611 Microbiol 19:1612-1624.
612 11. Ueno K, Nagamori A, Honkyu NO, Kataoka M, Shimizu K, Chang YC, Kwon-Chung KJ, Miyazaki Y.
613 2023. Cryptococcus neoformans requires the TVF1 gene for thermotolerance and virulence.
614 Med Mycol 61.

615 12. Winski CJ, Qian Y, Mobashery S, Santiago-Tirado FH. 2022. An Atypical ABC Transporter Is
616 Involved in Antifungal Resistance and Host Interactions in the Pathogenic Fungus Cryptococcus
617 neoformans. mBio 13:e0153922.
618 13. Oliveira NK, Bhattacharya S, Gambhir R, Joshi M, Fries BC. 2022. Novel ABC Transporter
619 Associated with Fluconazole Resistance in Aging of Cryptococcus neoformans. J Fungi (Basel) 8.
620 14. Moreno A, Banerjee A, Prasad R, Falson P. 2019. PDR-like ABC systems in pathogenic fungi. Res
621 Microbiol 170:417-425.
622 15. Khunweeraphong N, Kuchler K. 2021. Multidrug Resistance in Mammals and Fungi-From MDR to
623 PDR: A Rocky Road from Atomic Structures to Transport Mechanisms. Int J Mol Sci 22.
624 16. Jankovic D, Liu Z, Gause WC. 2001. Th1- and Th2-cell commitment during infectious disease:
625 asymmetry in divergent pathways. Trends Immunol 22:450-7.
626 17. Stacey AR, Norris PJ, Qin L, Haygreen EA, Taylor E, Heitman J, Lebedeva M, DeCamp A, Li D,
627 Grove D, Self SG, Borrow P. 2009. Induction of a striking systemic cytokine cascade prior to peak
628 viremia in acute human immunodeficiency virus type 1 infection, in contrast to more modest
629 and delayed responses in acute hepatitis B and C virus infections. J Virol 83:3719-33.
630 18. McMichael AJ, Borrow P, Tomaras GD, Goonetilleke N, Haynes BF. 2010. The immune response
631 during acute HIV-1 infection: clues for vaccine development. Nat Rev Immunol 10:11-23.
632 19. Wozniak KL, Ravi S, Macias S, Young ML, Olszewski MA, Steele C, Wormley FL. 2009. Insights into
633 the mechanisms of protective immunity against Cryptococcus neoformans infection using a
634 mouse model of pulmonary cryptococcosis. PLoS One 4:e6854.
635 20. Wozniak KL, Hardison S, Olszewski M, Wormley FL, Jr. 2012. Induction of protective immunity
636 against cryptococcosis. Mycopathologia 173:387-94.
637 21. Chang CC, Harrison TS, Bicanic TA, Chayakulkeeree M, Sorrell TC, Warris A, Hagen F, Spec A,
638 Oladele R, Govender NP, Chen SC, Mody CH, Groll AH, Chen YC, Lionakis MS, Alanio A, Castaneda
639 E, Lizarazo J, Vidal JE, Takazono T, Hoenigl M, Alffenaar JW, Gangneux JP, Soman R, Zhu LP,
640 Bonifaz A, Jarvis JN, Day JN, Klimko N, Salmanton-Garcia J, Jouvion G, Meya DB, Lawrence D,
641 Rahn S, Bongomin F, McMullan BJ, Sprute R, Nyazika TK, Beardsley J, Carlesse F, Heath CH,
642 Ayanlowo OO, Mashedi OM, Queiroz-Telles Filho F, Hosseinipour MC, Patel AK, Temfack E, Singh
643 N, Cornely OA, Boulware DR, et al. 2024. Global guideline for the diagnosis and management of
644 cryptococcosis: an initiative of the ECMM and ISHAM in cooperation with the ASM. Lancet Infect
645 Dis doi:10.1016/S1473-3099(23)00731-4.
646 22. Rothe C, Sloan DJ, Goodson P, Chikafa J, Mukaka M, Denis B, Harrison T, van Oosterhout JJ,
647 Heyderman RS, Lalloo DG, Allain T, Feasey NA. 2013. A prospective longitudinal study of the
648 clinical outcomes from cryptococcal meningitis following treatment induction with 800 mg oral
649 fluconazole in Blantyre, Malawi. PLoS One 8:e67311.
650 23. Coelho C, Casadevall A. 2016. Cryptococcal therapies and drug targets: the old, the new and the
651 promising. Cell Microbiol 18:792-9.
652 24. Zhang J, Li L, Lv Q, Yan L, Wang Y, Jiang Y. 2019. The Fungal CYP51s: Their Functions, Structures,
653 Related Drug Resistance, and Inhibitors. Front Microbiol 10:691.
654 25. Pulendran B. 2004. Modulating TH1/TH2 responses with microbes, dendritic cells, and pathogen
655 recognition receptors. Immunol Res 29:187-96.
656 26. Qiu Y, Dayrit JK, Davis MJ, Carolan JF, Osterholzer JJ, Curtis JL, Olszewski MA. 2013. Scavenger
657 receptor A modulates the immune response to pulmonary Cryptococcus neoformans infection. J
658 Immunol 191:238-48.
659 27. Brinks J, van Dijk EHC, Habeeb M, Nikolaou A, Tsonaka R, Peters HAB, Sips HCM, van de Merbel
660 AF, de Jong EK, Notenboom RGE, Kielbasa SM, van der Maarel SM, Quax PHA, Meijer OC, Boon
661 CJF. 2018. The Effect of Corticosteroids on Human Choroidal Endothelial Cells: A Model to Study
662 Central Serous Chorioretinopathy. Invest Ophthalmol Vis Sci 59:5682-5692.

663 28. Day J, Imran D, Ganiem AR, Tjahjani N, Wahyuningsih R, Adawiyah R, Dance D, Mayxay M,
664 Newton P, Phetsouvanh R, Rattanavong S, Chan AK, Heyderman R, van Oosterhout JJ, Chierakul
665 W, Day N, Kamali A, Kibengo F, Ruzagira E, Gray A, Lalloo DG, Beardsley J, Binh TQ, Chau TT,
666 Chau NV, Cuc NT, Farrar J, Hien TT, Van Kinh N, Merson L, Phuong L, Tho LT, Thuy PT, Thwaites
667 G, Wertheim H, Wolbers M. 2014. CryptoDex: a randomised, double-blind, placebo-controlled
668 phase III trial of adjunctive dexamethasone in HIV-infected adults with cryptococcal meningitis:
669 study protocol for a randomised control trial. Trials 15:441.
670 29. Kitonsa J, Nsubuga R, Mayanja Y, Kiwanuka J, Nikweri Y, Onyango M, Anywaine Z, Ggayi AB,
671 Kibengo FM, Kaleebu P, Day J. 2020. Determinants of two-year mortality among HIV positive
672 patients with Cryptococcal meningitis initiating standard antifungal treatment with or without
673 adjunctive dexamethasone in Uganda. PLoS Negl Trop Dis 14:e0008823.
674 30. Netea MG, Schlitzer A, Placek K, Joosten LAB, Schultze JL. 2019. Innate and Adaptive Immune
675 Memory: an Evolutionary Continuum in the Host's Response to Pathogens. Cell Host Microbe
676 25:13-26.
677 31. Rudman J, Evans RJ, Johnston SA. 2019. Are macrophages the heroes or villains during
678 cryptococcosis? Fungal Genet Biol 132:103261.
679 32. Hole C, Wormley FL, Jr. 2016. Innate host defenses against Cryptococcus neoformans. J
680 Microbiol 54:202-11.
681 33. Hole CR, Lam WC, Upadhya R, Lodge JK. 2020. Cryptococcus neoformans Chitin Synthase 3 Plays
682 a Critical Role in Dampening Host Inflammatory Responses. mBio 11.
683 34. O'Halloran JA, Powderly WG, Spec A. 2017. Cryptococcosis today: It is not all about HIV
684 infection. Curr Clin Microbiol Rep 4:88-95.
685 35. Koselny K, Mutlu N, Minard AY, Kumar A, Krysan DJ, Wellington M. 2018. A Genome-Wide
686 Screen of Deletion Mutants in the Filamentous Saccharomyces cerevisiae Background Identifies
687 Ergosterol as a Direct Trigger of Macrophage Pyroptosis. mBio 9.
688 36. Rodrigues ML. 2018. The Multifunctional Fungal Ergosterol. mBio 9.
689 37. Pasrija R, Panwar SL, Prasad R. 2008. Multidrug transporters CaCdr1p and CaMdr1p of Candida
690 albicans display different lipid specificities: both ergosterol and sphingolipids are essential for
691 targeting of CaCdr1p to membrane rafts. Antimicrob Agents Chemother 52:694-704.
692 38. Xu X, Bittman R, Duportail G, Heissler D, Vilcheze C, London E. 2001. Effect of the structure of
693 natural sterols and sphingolipids on the formation of ordered sphingolipid/sterol domains
694 (rafts). Comparison of cholesterol to plant, fungal, and disease-associated sterols and
695 comparison of sphingomyelin, cerebrosides, and ceramide. J Biol Chem 276:33540-6.
696 39. Upadhya R, Lam WC, Hole CR, Vasselli JG, Lodge JK. 2023. Cell wall composition in Cryptococcus
697 neoformans is media dependent and alters host response, inducing protective immunity. Front
698 Fungal Biol 4.
699 40. Kozel TR, Levitz SM, Dromer F, Gates MA, Thorkildson P, Janbon G. 2003. Antigenic and
700 biological characteristics of mutant strains of Cryptococcus neoformans lacking capsular O
701 acetylation or xylosyl side chains. Infect Immun 71:2868-75.
702 41. Posteraro B, Sanguinetti M, Sanglard D, La Sorda M, Boccia S, Romano L, Morace G, Fadda G.
703 2003. Identification and characterization of a Cryptococcus neoformans ATP binding cassette
704 (ABC) transporter-encoding gene, CnAFR1, involved in the resistance to fluconazole. Mol
705 Microbiol 47:357-71.
706 42. Prasad R, De Wergifosse P, Goffeau A, Balzi E. 1995. Molecular cloning and characterization of a
707 novel gene of Candida albicans, CDR1, conferring multiple resistance to drugs and antifungals.
708 Curr Genet 27:320-9.
709 43. Lamping E, Baret PV, Holmes AR, Monk BC, Goffeau A, Cannon RD. 2010. Fungal PDR
710 transporters: Phylogeny, topology, motifs and function. Fungal Genet Biol 47:127-42.

711 44. Del Poeta M, Wormley FL, Jr., Lin X. 2023. Host populations, challenges, and commercialization
712 of cryptococcal vaccines. PLoS Pathog 19:e1011115.
713 45. Wang Y, Wang K, Rivera A, Xue C. 2023. Development of a Heat-Killed fbp1 Mutant Strain as a
714 Therapeutic Agent To Treat Invasive Cryptococcus Infection. Microbiol Spectr 11:e0495522.
715 46. Pham T, Li Y, Watford W, Lin X. 2023. Vaccination with a ZNF2(oe) Strain of Cryptococcus
716 Provides Long-Lasting Protection against Cryptococcosis and Is Effective in
717 Immunocompromised Hosts. Infect Immun 91:e0019823.
718 47. Wormley FL, Jr., Perfect JR, Steele C, Cox GM. 2007. Protection against cryptococcosis by using a
719 murine gamma interferon-producing Cryptococcus neoformans strain. Infect Immun 75:1453-
720 62.
721 48. Ristow LC, Jezewski AJ, Chadwick BJ, Stamnes MA, Lin X, Krysan DJ. 2023. Cryptococcus
722 neoformans adapts to the host environment through TOR-mediated remodeling of phospholipid
723 asymmetry. Nat Commun 14:6587.
724 49. Santiago-Tirado FH, Peng T, Yang M, Hang HC, Doering TL. 2015. A Single Protein S-acyl
725 Transferase Acts through Diverse Substrates to Determine Cryptococcal Morphology, Stress
726 Tolerance, and Pathogenic Outcome. PLoS Pathog 11:e1004908.
727 50. Santiago-Tirado FH, Hurtaux T, Geddes-McAlister J, Nguyen D, Helms V, Doering TL, Romisch K.
728 2023. The ER Protein Translocation Channel Subunit Sbh1 Controls Virulence of Cryptococcus
729 neoformans. mBio 14:e0338422.
730 51. Gish SR, Maier EJ, Haynes BC, Santiago-Tirado FH, Srikanta DL, Ma CZ, Li LX, Williams M, Crouch
731 EC, Khader SA, Brent MR, Doering TL. 2016. Computational Analysis Reveals a Key Regulator of
732 Cryptococcal Virulence and Determinant of Host Response. mBio 7:e00313-16.

733

734

735

736

737

738

739

740

741

742

743

744

745

746

747 **Figures and figure legends**

748

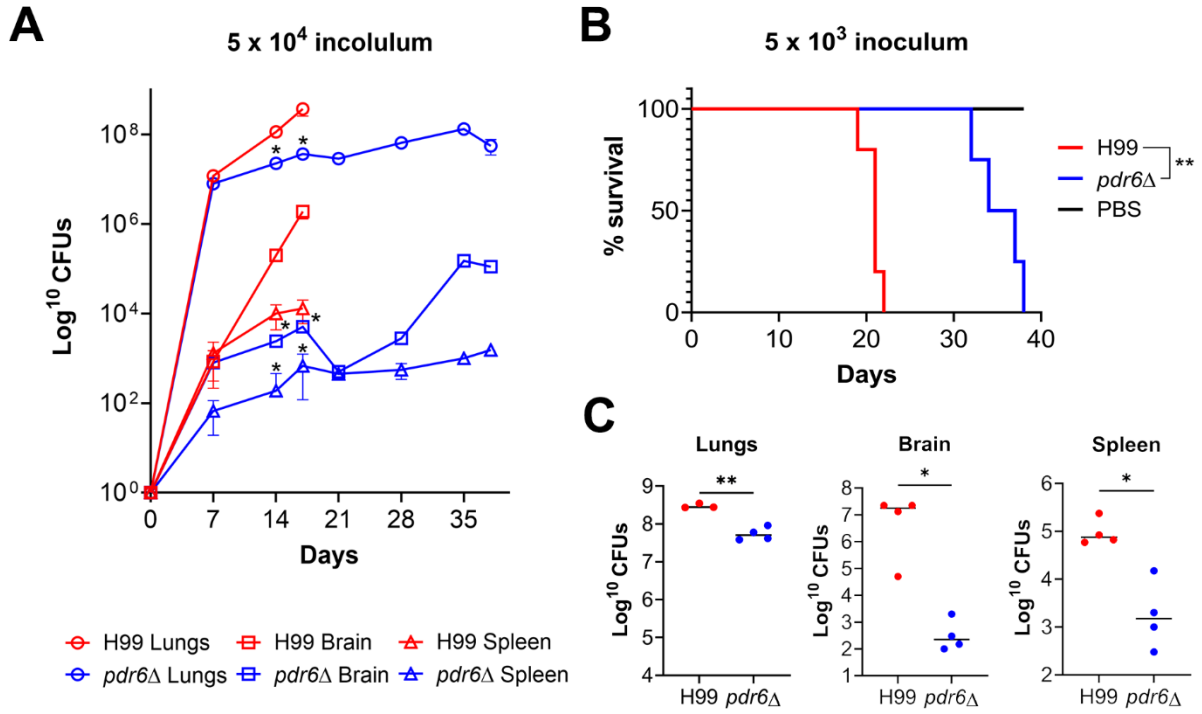

749

750 **Fig. 1. *C. neoformans pdr6*Δ-infected mice succumb to infection despite decreased fungal**
751 **burden. (A)** Quantified fungal burden over time to monitor disease progression. Mice were
752 inoculated with 5 x 10^4 cells and sacrificed every 7 days and organs were harvested to
753 determine CFUs. Significance was determined using Mann-Whitney test, *P<0.05. **(B)** In vivo
754 survival of H99 and *pdr6*Δ strains. 4 A/J mice per group were intranasally infected with 5 x 10^3
755 cryptococcal cells or mock infected with sterile PBS and monitored for 38 days (experiment was
756 terminated when the last infected mouse reached endpoint). Significance was determined
757 using Mantel-Cox test, **P<0.01. **(C)** Quantified organ burdens of H99 and *pdr6*Δ-infected mice
758 at TOD. Organs were harvested, homogenized, and dilutions were plated on YPD. Plates were
759 incubated for 48 h and CFUs were counted. Each data point represents a mouse and black bars
760 represent the mean. Significance was determined using Mann-Whitney test, *P<0.05; **P<0.01.

761

762

763

764

765

766

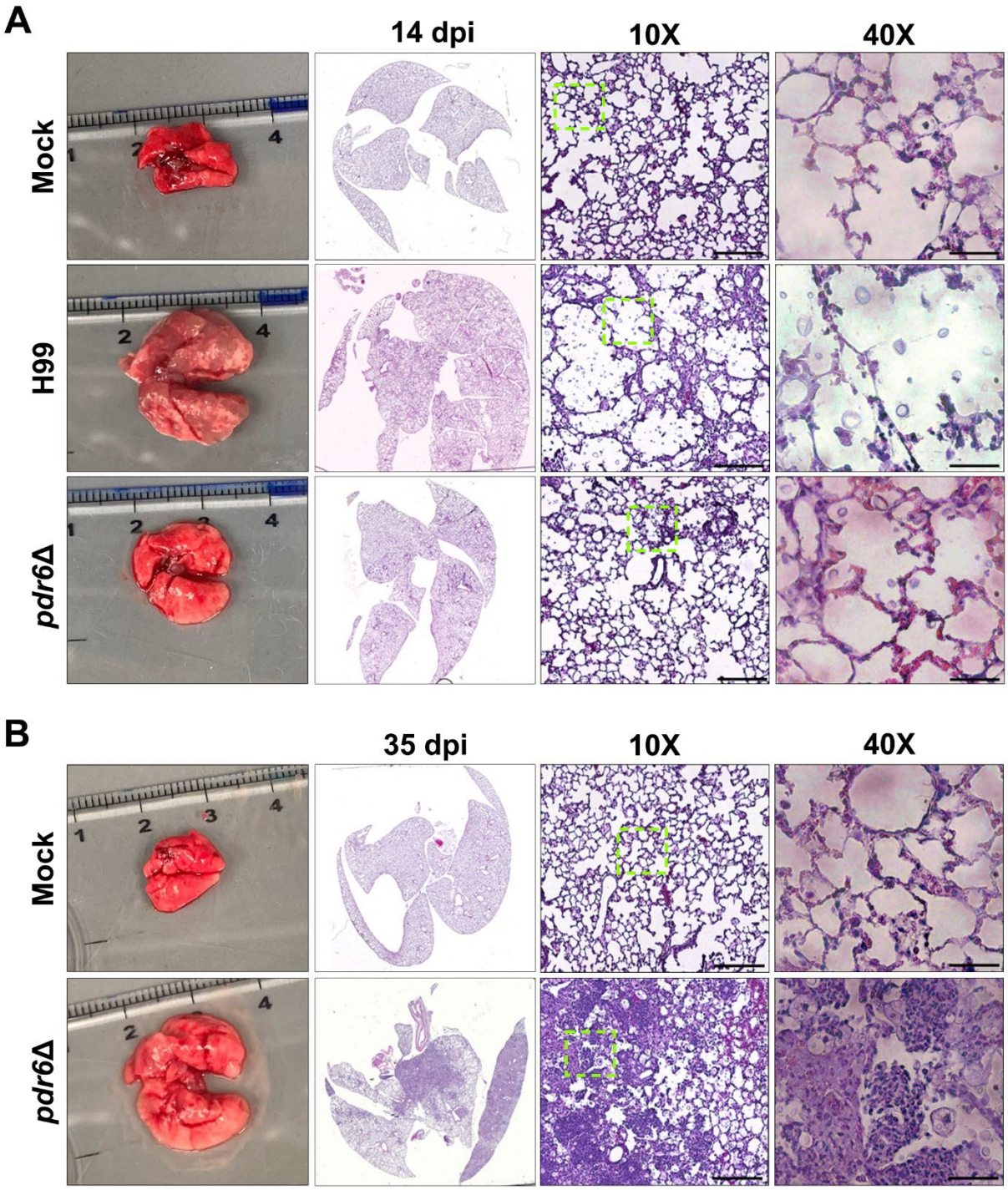

Fig. 2. Infection with *C. neoformans pdr6Δ* results in altered histopathology. (A & B) Dissected lungs of female A/J mice infected with 5 x 10^4 cells of the WT strain or *pdr6*Δ mutant strain were harvested at predetermined endpoints of 14 **(A)** and 35 **(B)** dpi. Gross organ examination revealed significant changes in inflammation and tissue damage. H&E staining was used to

772 visualize microscopic lung pathology (inset [green boxes]). The 10X scale bar is 200 μm and the
773 40X scale bar is 50 μm.

774

DPI	Strain	% inflammation	Fungal infiltration	Quantitation of inflammatory immune cells/hpf 400X	Observations
7	H99	5 – 10%	20% alveoli contain encapsulated yeast	8 neutrophils 33 lymphocytes 40 histiocytes	Immune cells in peri-bronchial and perivascular space.
	*pdr6*Δ	5 – 10%	15 – 20% alveoli contain encapsulated yeast	9 neutrophils 26 lymphocytes 19 histiocytes	Immune cells in peri-bronchial and perivascular space. Some yeast has been phagocytized by histiocytes.
14	H99	10%	80 – 90% alveoli contain encapsulated yeast	52 neutrophils 26 lymphocytes 57 histiocytes	Immune cells in peri-bronchial and perivascular space.
	*pdr6*Δ	10%	50 – 60% alveoli contain encapsulated yeast	43 neutrophils 105 lymphocytes 71 histiocytes	Immune cells in peri-bronchial and perivascular space. Many histiocytes have phagocytized yeast. Areas of accumulated yeast/immune cells but no true parenchymal granulomas.
21*	*pdr6*Δ	10%	90% alveoli contain encapsulated yeast	50 neutrophils 49 lymphocytes 55 histiocytes	Immune cells in peri-bronchial and perivascular space.
28*	*pdr6*Δ	5 – 10%	80% alveoli contain encapsulated yeast	8 neutrophils 33 lymphocytes 55 histiocytes	Immune cells in peri-bronchial and perivascular space and single parenchymal granuloma (1.2mm)
35*	*pdr6*Δ	60 – 70%	100% present throughout	Too many to quantify	Consolidated parenchyma with many coalescent granulomas (histiocytes w/phagocytized yeast) and nests of neutrophils and lymphocytes with necrosis.

775

776 **Table 1. Quantitative analysis of H99 and *pdr6*Δ-infected lung sections over time.**
777 *All H99-infected mice had succumbed to infection by timepoint.
778 Histiocytes refer to leukocytes of the monocyte/macrophage/dendritic cell lineage.
779 hpf, high power field.
780

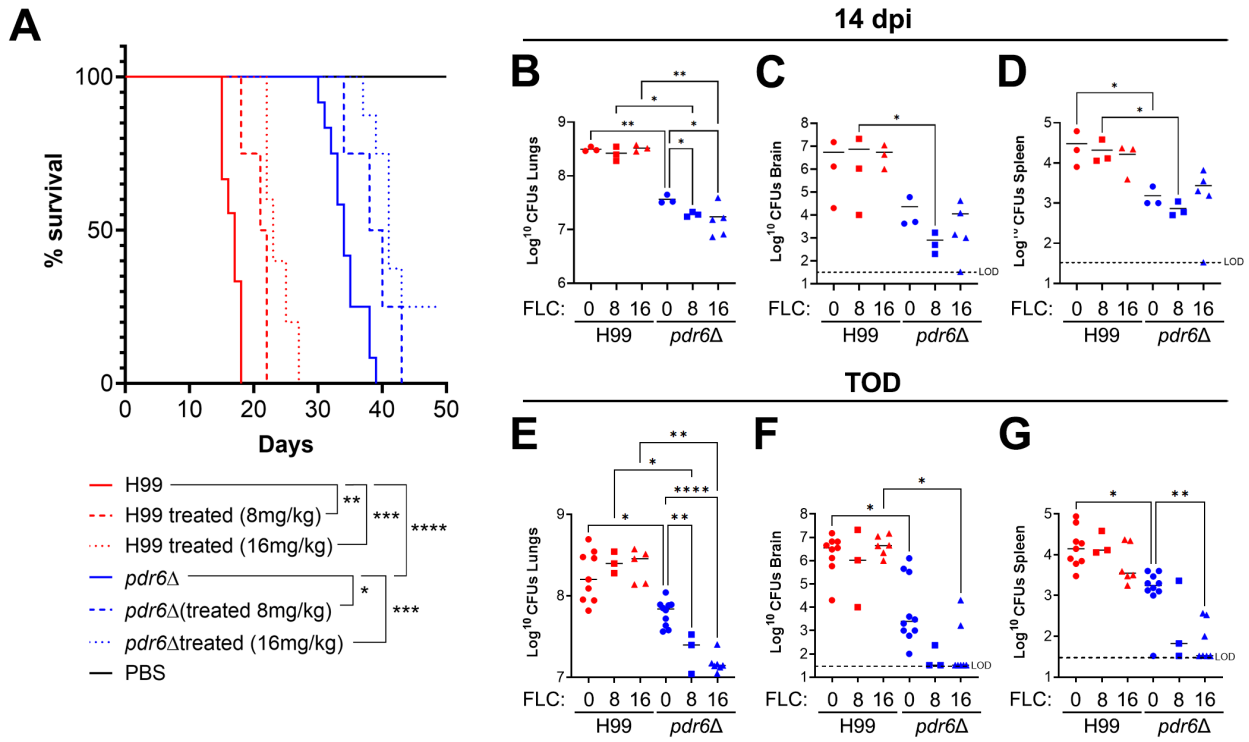

Fig. 3. FLC treatment significantly reduces CFUs in *pdr6*Δ-infected mice. (A) *In vivo* survival curve of H99 and *pdr6*Δ-infected mice treated daily with either 8 or 16 mg/kg FLC. At least 4 A/J mice per group were intranasally infected with 5 x 10^4 cells, or mock-infected with DPBS and monitored for up to 50 dpi (mock-infected and FLC-treated mice not shown for clarity). Significance was determined using Mantel-Cox test, *P<0.05; **P<0.01; ***P<0.001; ****P<0.0001. **(B-G)** Calculated organ burdens at 14 dpi **(B-D)** or endpoint **(E-G)**. Organs were harvested, homogenized, and dilutions were plated on YPD. Plates were incubated for 48 hr and CFUs were enumerated. Each data point represents a mouse and black bars represent the mean. Significance was determined using one-way ANOVA with multiple comparisons (Welch's corrected) *P<0.05; **P<0.01; ****P<0.0001.

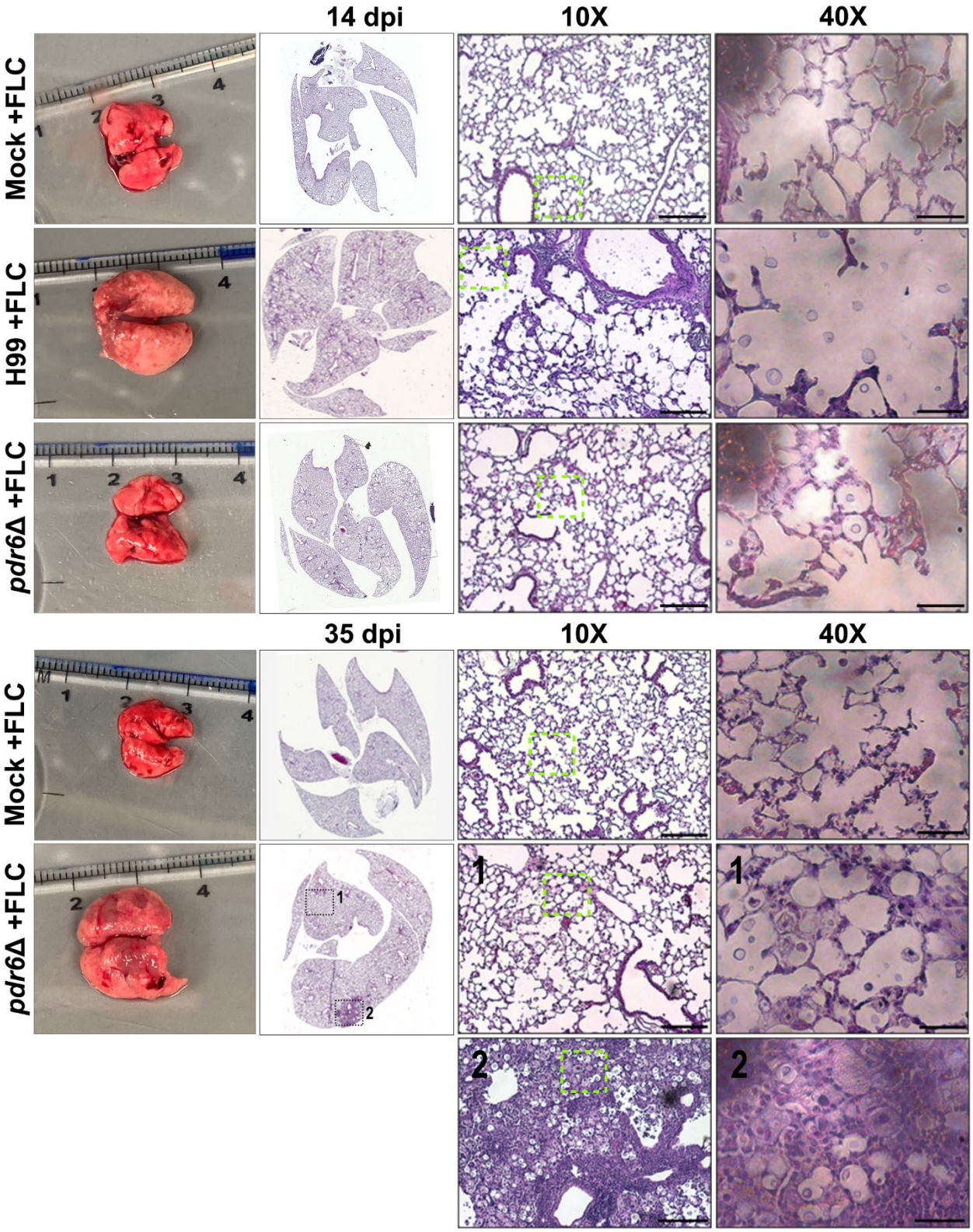

793

794 **Fig. 4. FLC treatment improves lung pathology in *pdr6*Δ-infected animals.** Dissected lungs of
795 female A/J mice infected with 5 x 10^4 cells of the WT strain or *pdr6*Δ mutant strain and treated

796 daily with 16 mg/kg FLC were harvested at 14 and 35 dpi. Gross organ examination revealed
797 alterations in fungal containment and disease progression. H&E staining was used to visualize
798 microscopic lung pathology. Insets 1 & 2 highlight differential histopathology in the FLC-treated
799 *pdr6*Δ-infected mice at 35 dpi (inset [green boxes]). Inset 1 shows an intact lung parenchyma
800 with several fungi and immune cells while inset 2 is characterized as a granuloma. The 10X scale
801 bar is 200 μm and the 40X scale bar is 50 μm.

802

DPI	Strain	% inflammation	Fungal infiltration	Quantitation of inflammatory immune cells/hpf 400X	Observations
14	Mock +FLC	0%	None	-	-
	H99 +FLC	5 – 10%	~ 60% alveoli contain encapsulated yeast	50 – 60 neutrophils 40 – 50 lymphocytes 15 histiocytes	Moderate number of inflammatory cells predominately present in perivascular & peribronchial areas.
	*pdr6*Δ +FLC	< 5%	30 – 40% alveoli contain encapsulated yeast	1 – 5 neutrophils 0 – 15 lymphocytes 1 – 5 histiocytes	Mild infiltrate of inflammatory cells in focal peribronchial & perivascular areas.
35	Mock +FLC	0%	None	-	-
	*pdr6*Δ +FLC	5 – 10%	45 – 50% alveoli contain encapsulated yeast	5 – 10 neutrophils 10 – 20 lymphocytes < 5 histiocytes	Mild inflammatory cell infiltrate in many peribronchial and perivascular areas. Consolidation of adjacent alveoli in solid areas.

803

804 **Table 2. Quantitative analysis of Fluconazole treated H99 and *pdr6*Δ-infected lung sections**
805 **over time**
806 Histiocytes refer to leukocytes of the monocyte/macrophage/dendritic cell lineage.
807 hpf, high power field.
808

809

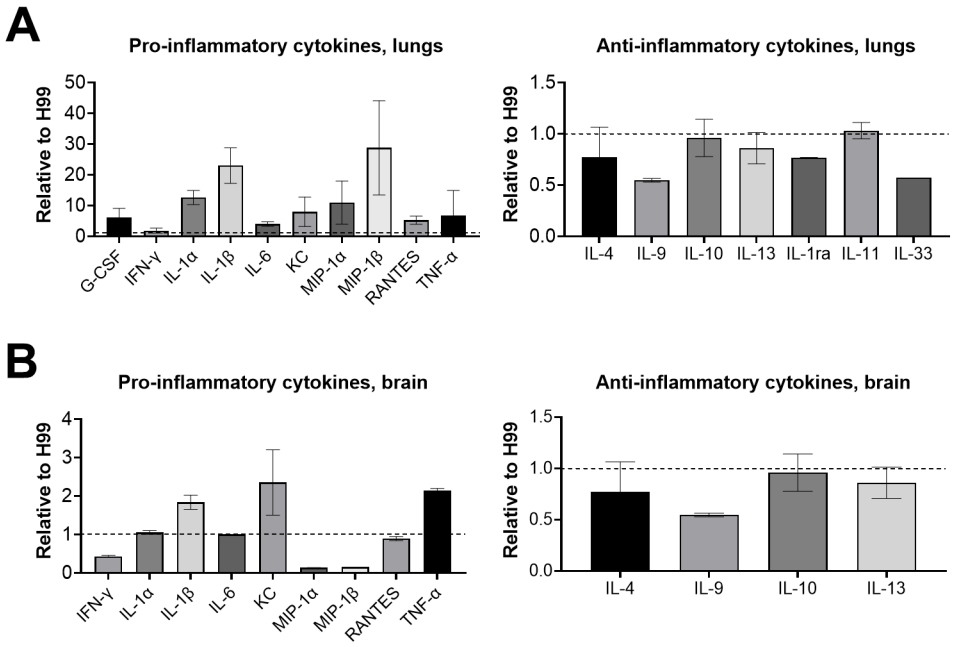

Fig. 5 Infection with the *pdr6*Δ mutant elicits a robust pro-inflammatory immune response. (A & B) Quantification of pro-inflammatory and anti-inflammatory cytokines in the lungs **(A)** and brains **(B)** of *C. neoformans*-infected mice. Female A/J mice were intranasally infected with 5 x 10^5 cells of the H99 or *pdr6*Δ strain and euthanized at endpoint. Homogenates from the lungs and brain were used to perform Proteome Profiler Mouse XL Cytokine Arrays and Bio-Plex Multi-Plex Arrays. Expression of cytokines/chemokines in *pdr6*Δ-infected mice was normalized to H99 (dotted line).

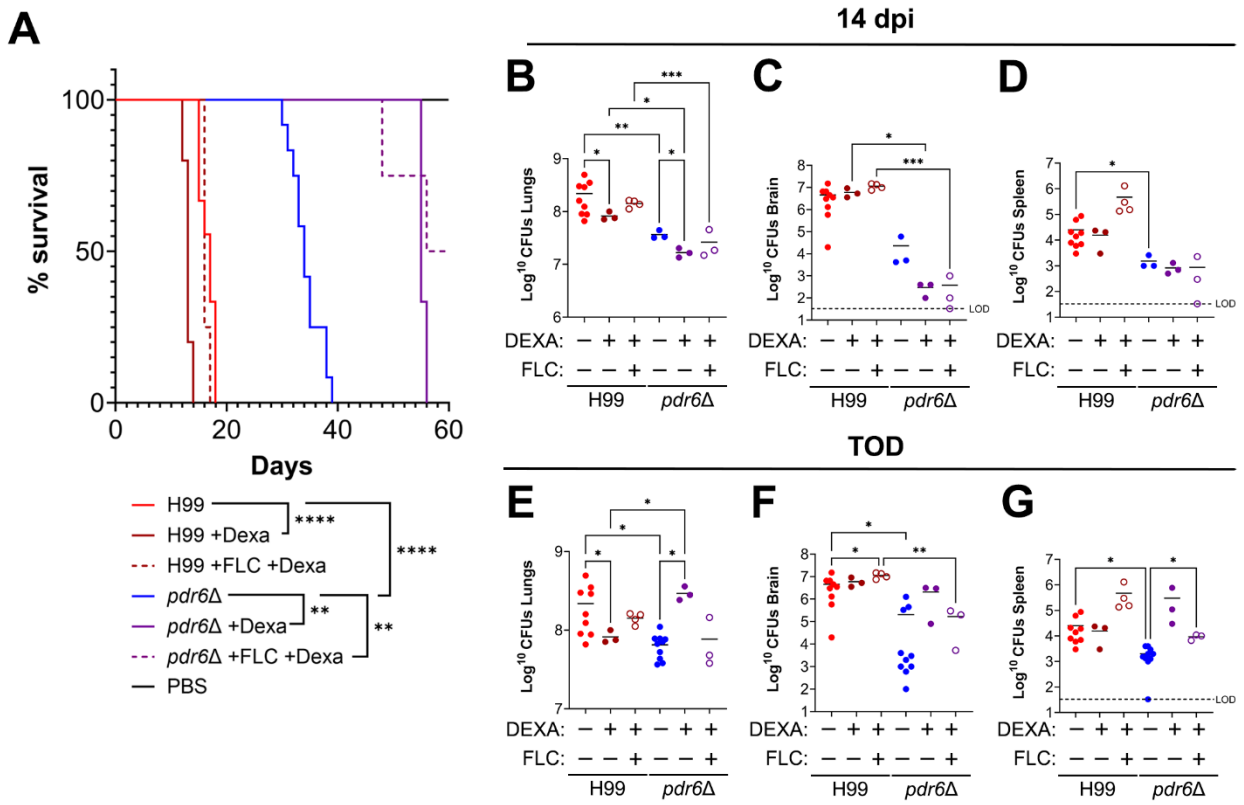

Fig. 6 Dexamethasone treatment significantly extends survival in *pdr6*Δ-infected mice. (A) *In vivo* survival curve of H99 and *pdr6*Δ-infected mice treated daily with either 0.03 mg/kg Dexa or 0.03 mg/kg Dexa and 16 mg/kg FLC. At least 3 A/J mice per group were intranasally infected with 5 x 10^4 cells, or mock-infected with DPBS and monitored for up to 60 dpi (mock-infected and treated mice not shown for clarity). Significance was determined using Mantel-Cox test, **P<0.01; ****P<0.0001. **(B-G)** Calculated organ burdens at 14 dpi **(B-D)** or endpoint **(E-G)**. Organs were harvested, homogenized, and dilutions were plated on YPD. Plates were incubated for 48 hr and CFUs were enumerated. Each data point represents a mouse and black bars represent the mean. Significance was determined using one-way ANOVA with multiple comparisons (Welch's corrected) *P<0.05; **P<0.01; ***P<0.001.

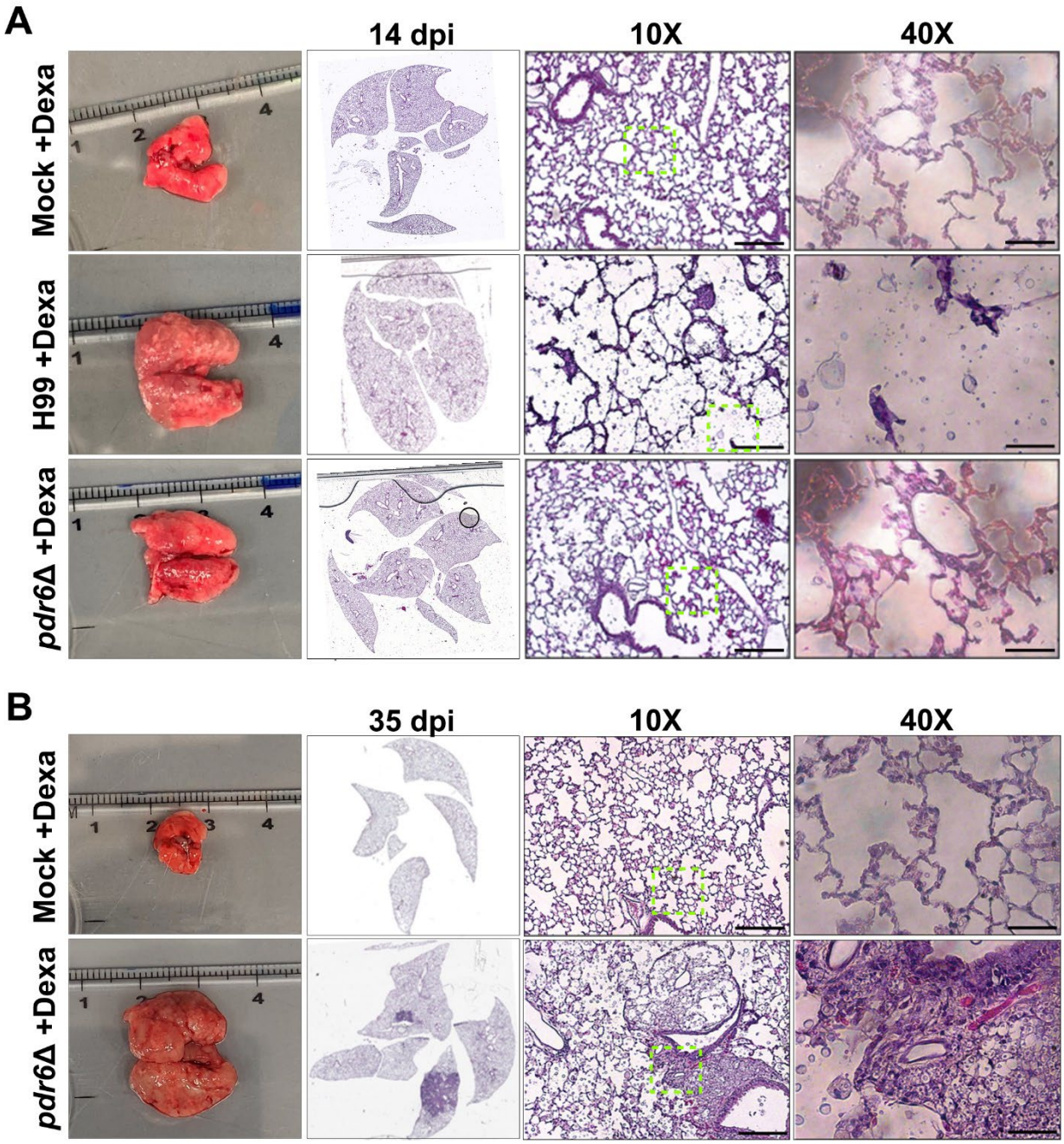

Fig. 7. Effect of dexamethasone treatment on lung histopathology. Dissected lungs of female A/J mice infected with 5 x 10^4 cells of the WT strain or *pdr6*Δ mutant strain and treated daily with 0.3 mg/kg Dexa and harvested at 14 and 35 dpi. Gross organ examination revealed alterations inflammation. H&E staining was used to visualize microscopic lung pathology (inset [green boxes]). The 10X scale bar is 200 μm and the 40X scale bar is 50 μm.

838

DPI	Strain	% inflammation	Fungal infiltration	Quantitation of inflammatory immune cells/hpf 400X	Observations
14	Mock +Dexa	0%	None	-	-
	H99 +Dexa	10%	85 – 90% alveoli contain encapsulated yeast	10 – 20 neutrophils 10 – 30 lymphocytes < 5 histiocytes	Perivascular and peribronchial aggregates of admixed neutrophils and lymphocytes.
	*pdr6*Δ +Dexa	< 5%	20 – 30% alveoli contain encapsulated yeast	5 – 10 neutrophils 5 lymphocytes < 5 histiocytes	Focal inflammatory cell nests in perivascular and peribronchial space.
50	Mock +Dexa	0%	None	-	Inflammatory cells uncommon. Rare small nests of lymphocytes on or near pleural surface.
	*pdr6*Δ +Dexa	20%	> 80% alveoli contain encapsulated yeast	5 – 10 neutrophils 5 – 10 lymphocytes 20 – 30 histiocytes	Focal consolidated areas of dense inflammatory tissue up to 4 – 5 mm in dimension.

839 **Table 3. Quantitative analysis of Dexamethasone treated H99 and *pdr6*Δ-infected lung**
840 **sections over time**
841 Histiocytes refer to leukocytes of the monocyte/macrophage/dendritic cell lineage.
842 hpf, high power field.
843

844

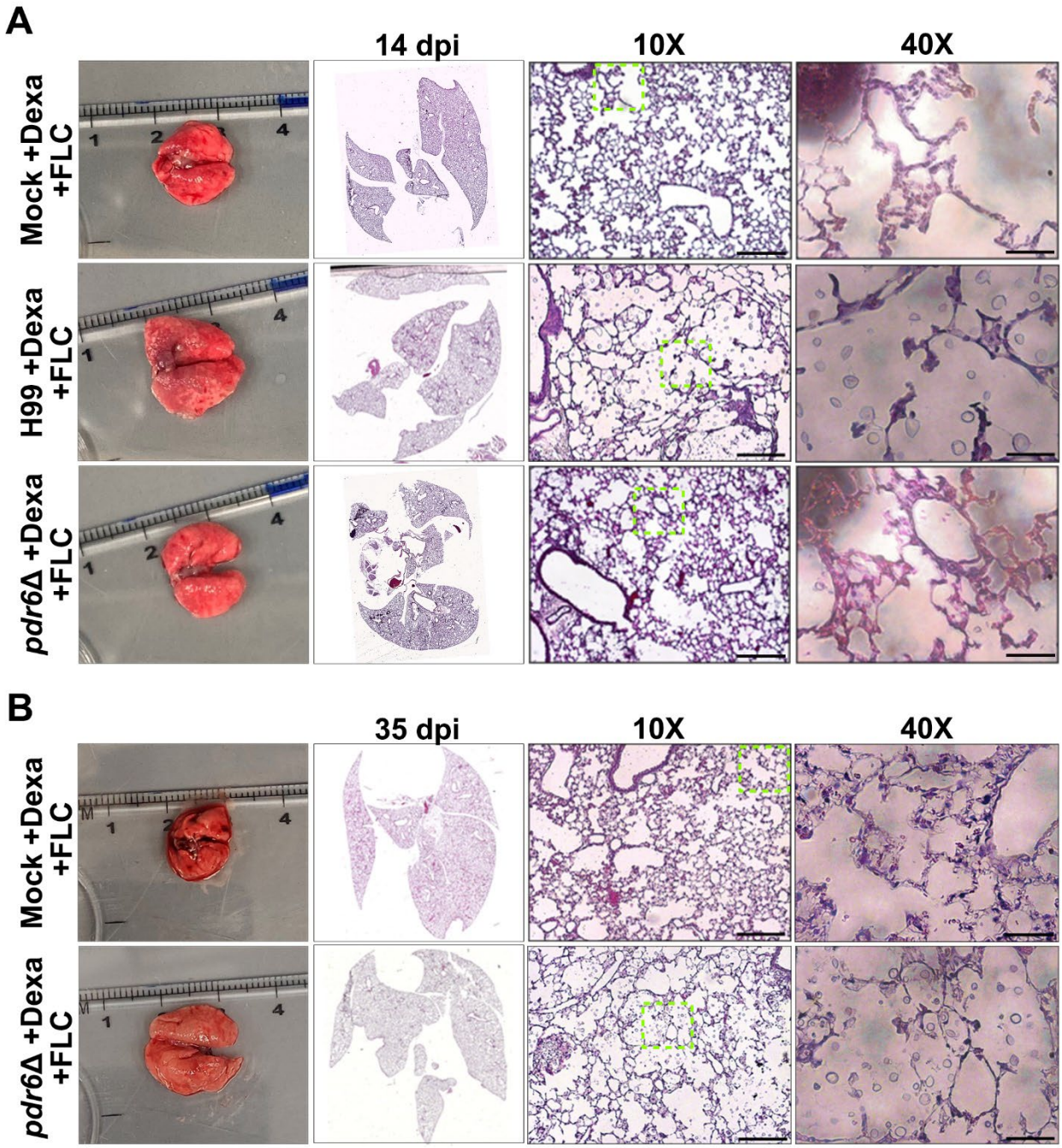

845

846 **Fig. 8. Effect of dexamethasone/FLC combination treatment on lung histopathology.**
847 Dissected lungs of female A/J mice infected with 5 x 10^4 cells of the WT strain or *pdr6*Δ mutant
848 strain and treated daily with a combination of 0.3 mg/kg Dexa and 16 mg/kg FLC and harvested
849 at 14 and 35 dpi. Gross organ examination revealed alterations inflammation. H&E staining was
850 used to visualize microscopic lung pathology (inset [green boxes]). The 10X scale bar is 200 μm
851 and the 40X scale bar is 50 μm.

852

DPI	Strain	% inflammation	Fungal infiltration	Quantitation of inflammatory immune cells/hpf 400X	Observations
14	Mock +Dexa +FLC	0%	None	-	-
	H99 +Dexa +FLC	15 – 20%	45 – 50% alveoli contain encapsulated yeast	15 – 30 neutrophils 15 – 30 lymphocytes < 5 histiocytes	Small to medium sized nests of inflammatory cells.
	*pdr6*Δ +Dexa +FLC	0%	10 – 15% alveoli contain encapsulated yeast	-	Inflammatory cells are uncommon with rare perivascular and peribronchial nests of small lymphocytes and few histiocytes.
50	Mock +Dexa +FLC	0%	None	Rare clusters of 2 – 4 histiocytes	Mildly dilated capillaries.
	*pdr6*Δ +Dexa +FLC	0%	75 – 80% alveoli contain encapsulated yeast	-	Few small foci of perivascular lymphocytes and rare histiocytes.

853

854 **Table 4. Quantitative analysis of combination Dexamethasone + Fluconazole treated H99 and**
855 ***pdr6*Δ-infected lung sections over time**
856 Histiocytes refer to leukocytes of the monocyte/macrophage/dendritic cell lineage.
857 hpf, high power field.
858

859

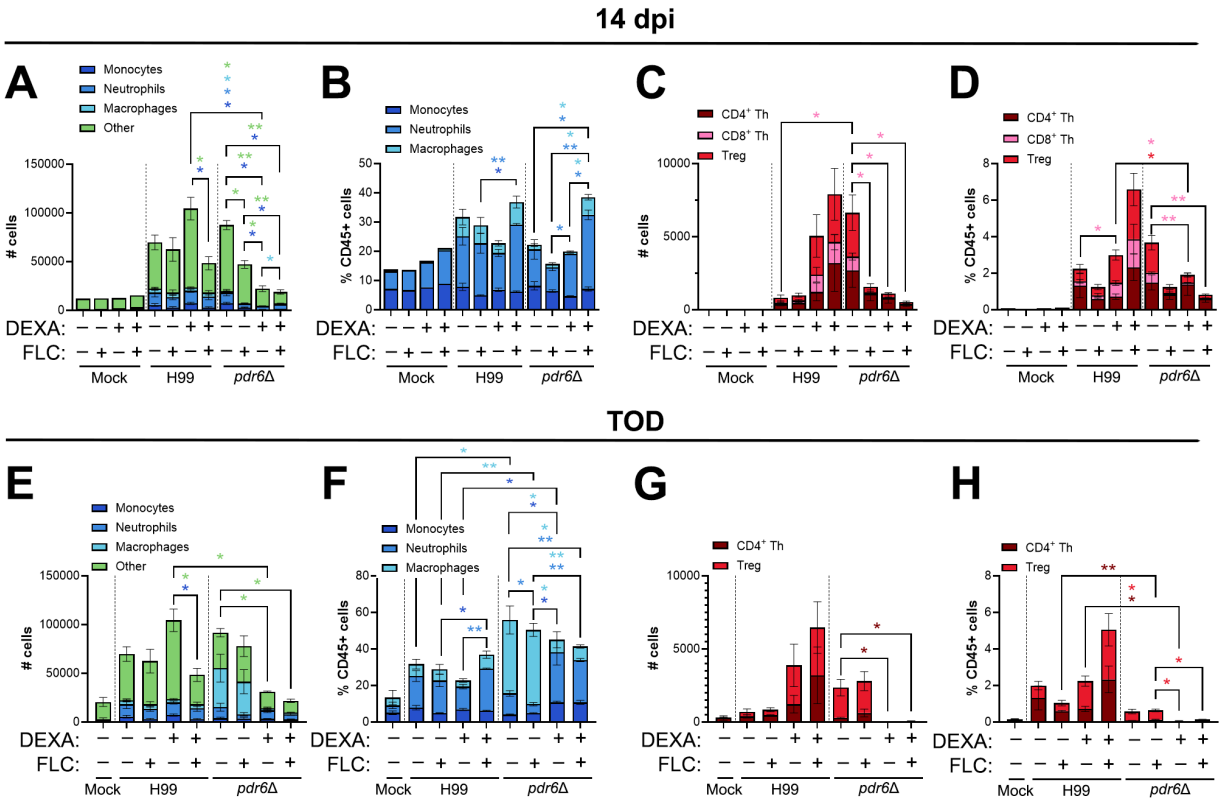

Fig. 9 Infection with the *C. neoformans pdr6Δ* mutant generates an increase in innate immune cells, specifically macrophages. (A-H) Quantification of innate and adaptive immune cell populations at 14 dpi **(A-D)** and endpoint **(E-H)**. Female A/J mice were intranasally infected with 5 x 10^4 cells of the H99 or *pdr6*Δ strain and euthanized at clinical endpoints corresponding to imminent mortality. Lungs were harvested and single-cell suspensions were generated and stained with immune panels to quantify monocytes, neutrophils, macrophages, $CD4^+$ Th, $CD4^+$ T-regs, and $CD8^+$ cells. Samples were processed using flow cytometry and are presented as total # cells **(A, C, E, G)** or as % $CD45^+$ cells **(B, D, F, H)**. Significance was determined using one-way ANOVA with multiple comparisons (Welch's corrected) *P<0.05; **P<0.01. Note: for **G** and **H**, the $CD8^+$ T cell panel could not be run for the day 35 samples, hence they were removed from the H99 bars.

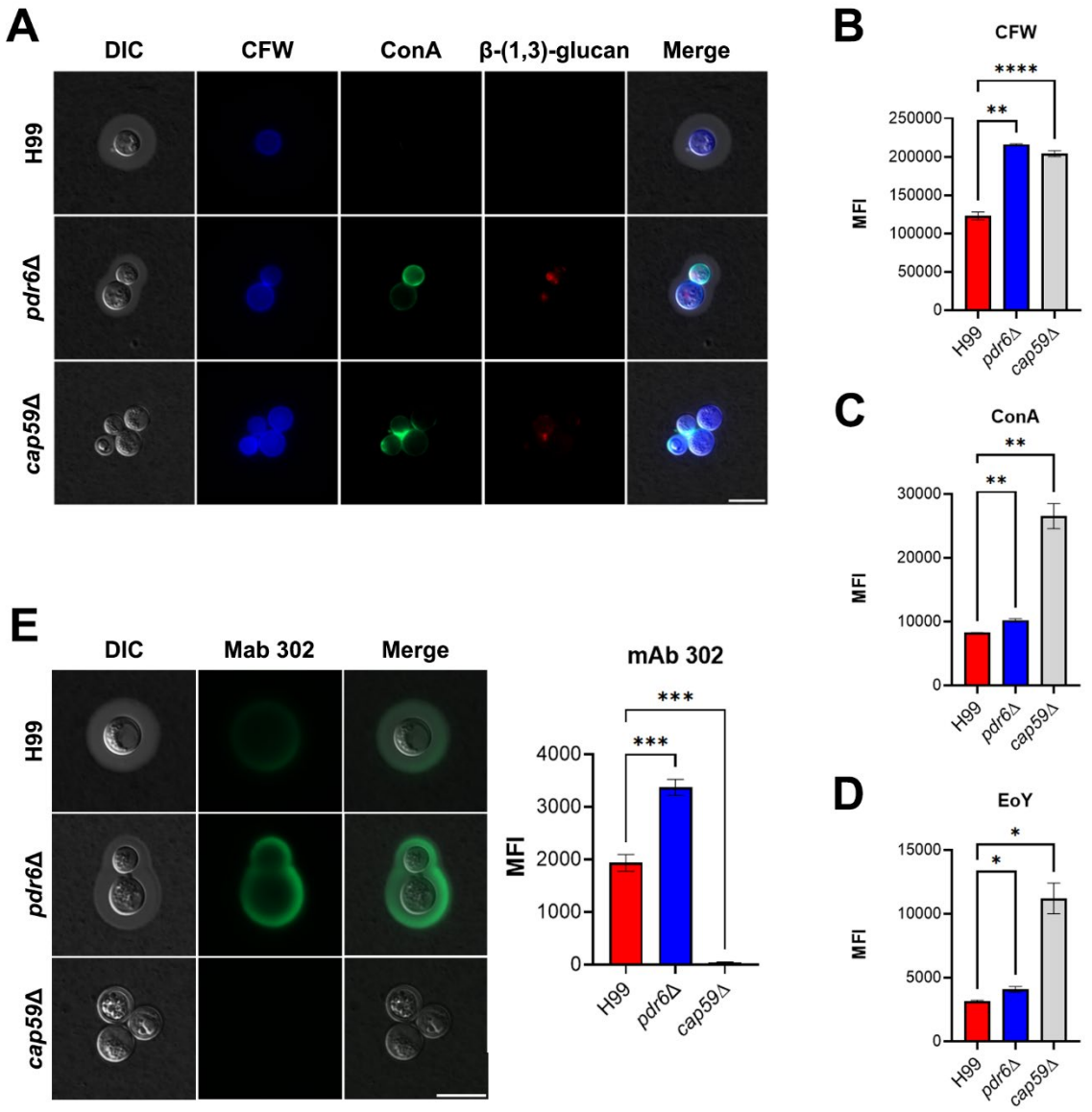

Fig. 10 *C. neoformans pdr6*Δ cells display increased PAMP exposure and altered capsule density. (A) Visualization of CFW, ConA, and β-(1,3)-glucan staining in H99, *pdr6*Δ, and *cap59*Δ cells. Representative images of stained cells. Scale bar, 10 μm. **(B)** Quantification of CFW, ConA, and EoY in H99, *pdr6*Δ, and *cap59*Δ strains. Cells were stained and measured using flow cytometry. Significance was determined using one-way ANOVA (Welch's corrected) *P<0.05; **P<0.01; ****P<0.0001. **(C)** Visualization and quantification of capsular antibody staining of H99, *pdr6*Δ, and *cap59*Δ strains. Cells were stained with anti-capsule mAb 302 and imaged using an inverted Zeiss microscope. Representative images of stained cells. Staining was quantified using a Cell Profiler pipeline. Significance was determined using one-way ANOVA (Welch's corrected) ***P<0.001.